nature methods

Article

https://doi.org/10.1038/s41592-023-02037-0

Hydrogel-based molecular tension fluorescence microscopy for investigating receptor-mediated rigidity sensing

Received: 31 October 2022

Accepted: 5 September 2023

Published online: 5 October 2023

Check for updates

Wenxu Wang[1,4], Wei Chen[1,4], Chaoyang Wu[1,4], Chen Zhang[2], Jingjing Feng[1], Pengxiang Liu[1], Yuru Hu[1], Hongyun Li[1], Feng Sun[1], Kai Jiang[3], Xinghua Zhang[2] & Zheng Liu[1,2]

Extracellular matrix (ECM) rigidity serves as a crucial mechanical cue impacting diverse biological processes. However, understanding the molecular mechanisms of rigidity sensing has been limited by the spatial resolution and force sensitivity of current cellular force measurement techniques. Here we developed a method to functionalize DNA tension probes on soft hydrogel surfaces in a controllable and reliable manner, enabling molecular tension fluorescence microscopy for rigidity sensing studies. Our findings showed that fibroblasts respond to substrate rigidity by recruiting more force-bearing integrins and modulating integrin sampling frequency of the ECM, rather than simply overloading the existing integrin–ligand bonds, to promote focal adhesion maturation. We also demonstrated that ECM rigidity positively regulates the pN force of T cell receptor–ligand bond and T cell receptor mechanical sampling frequency, promoting T cell activation. Thus, hydrogel-based molecular tension fluorescence microscopy implemented on a standard confocal microscope provides a simple and effective means to explore detailed molecular force information for rigidity-dependent biological processes.

As a major mechanical cue, extracellular matrix (ECM) rigidity has been demonstrated to influence many critical life processes, including stem cell differentiation[1], platelet activation[2] and tumor metastasis[3]. To understand how cells sense and respond to ECM stiffness, traction force microscopy (TFM) or micropost arrays have been widely applied to measure the mechanical force exerted by a cell adhering to a soft hydrogel surface[4]. For example, Prager-Khoutorsky et al. found that matrix stiffness may alter the polarization of fibroblasts by influencing the mechanotransduction of focal adhesions (FAs) in fibroblasts[5]. Plotnikov et al. utilized TFM to investigate the distribution and dynamics of traction forces generated by individual mature FAs on hydrogels with different stiffnesses and found that individual FAs can exert fluctuating traction forces on the ECM to probe the matrix rigidity and promote cell durotaxis[6]. Furthermore, after using TFM to study the complex relationship between hydrogel stiffness and cellular traction, researchers proposed that cells transmit and regulate FA-mediated mechanotransduction through an 'actin-adaptor protein–integrin–ECM' linkage, termed the molecular clutch[7–9]. Although TFM has greatly promoted the growth of the mechanobiology field, the coarser force sensitivity (nanonewton) and ~micron spatial image resolution of TFM probably limit our understanding of the molecular mechanisms of rigidity sensing, that is, the ability of the cell to sense and respond to the stiffness of its environment.

[1]TaiKang Center for Life and Medical Sciences, the Institute for Advanced Studies, Wuhan University, Wuhan, China. [2]College of Life Sciences, Wuhan University, Wuhan, China. [3]Frontier Science Center for Immunology and Metabolism, Medical Research Institute, Wuhan University, Wuhan, China. [4]These authors contributed equally: Wenxu Wang, Wei Chen, Chaoyang Wu. e-mail: zheng.liu@whu.edu.cn

Stabley et al. have recently pioneered the invention of molecular tension fluorescence microscopy (mTFM)[10], a technology that employs immobilized mechanosensitive fluorescent molecular probes to image and quantify pN-level forces experienced by live cell membrane receptors. Using mTFM, researchers were able to image the molecular forces of transmembrane receptors such as integrins[11,12] and T cell receptors (TCRs)[13,14] in living cells in real time, and revealed that ~pN level forces transmitted through the individual receptors mediated cell adhesion and T cell activation. Recently, our group developed a reversible shearing DNA-based tension probe (RSDTP)[15] that expands the range of force measurements of reversible molecular tension probes and revealed that mechanically strong integrins (>56 pN) maintained FA maturation. Although mTFM can measure cellular force at the molecular level, the technique is currently limited to the study of cells spreading on coverslips[16] or lipid bilayers[17] that are mechanically different from soft ECM. To the best of our knowledge, it is currently difficult to map the molecular force during rigidity sensing using mTFM mainly due to the complex chemical and physical structural properties of hydrogel that make it challenging to specifically modify molecular tension probes on its surface.

In this Article, we have developed an experimental procedure to functionalize DNA tension probes on soft hydrogel surfaces in a controllable and reliable manner. In addition, fluorescent nanospheres were conjugated on the same hydrogel surface, which allowed us to couple the mTFM with conventional TFM and gather more comprehensive data, including molecular force mapping, net cell traction and force orientation. Using hydrogel-based mTFM, we investigated how ECM stiffness regulates receptor-mediated force transmission processes. We found that fibroblasts respond to substrate rigidity primarily by recruiting more force-bearing integrins and modulating the frequency at which integrins sample the ECM rather than by increasing the average magnitude of integrin forces of FAs. Moreover, we discovered that ECM rigidity has a positive impact on the pN forces involved in TCR–ligand interaction and TCR mechanical scanning dynamics, which ultimately promotes the efficiency of T cell activation in response to antigen recognition. Our results demonstrated that hydrogel-based mTFM can be used to study mechanotransduction processes of cells spreading on soft hydrogels, which are mechanically more similar to tissues, and may provide novel insights into the molecular mechanisms underlying cell rigidity sensing and mechanotransduction.

Results

Hydrogel-based mTFM development for cellular force imaging

Unlike glass or lipid layers, hydrogels are highly porous and heterogeneous[1]. Thus, if the molecular tension probes were directly crosslinked with hydrogel materials, the majority will be absorbed by the inner hydrogel matrix as notable background signal during imaging, which would override the real mTFM signal on the surface and pose a challenge to obtaining high-quality mTFM maps on hydrogels. Here we have developed an experimental procedure for the selective modification of gold nanoparticle (Au NP)-based tension sensors[13,15,18] on the hydrogel surface (Fig. 1a, Extended Data Figs. 1–5 and Supplementary Figs. 1–4). Briefly, we first covalently attached DNA-based tension probes to Au NPs, specifically by freezing their mixture at −80 °C for 1 h to achieve a high DNA density and good colloidal stability of DNA–Au NPs hybrid[19]. The DNA–Au NPs hybrid colloid was then incubated with a lipoic acid-functionalized polyacrylamide (PA) hydrogel 30 min to form stable crosslinks of hydrogel–Au NPs–DNA (Extended Data Fig. 2). Notably, the tension probes were primarily immobilized on the hydrogel surface because the physical size of the preassembled Au NP–DNA tension probe complex can prevent its penetration into the hydrogel matrix. Therefore, the background noise generated by the probes inside the hydrogel matrix could be substantially reduced. Optionally, fluorescent nanobeads could be conjugated with the same hydrogel surface (Fig. 1a and Extended Data Fig. 2), thus allowing us to couple the mTFM with conventional TFM and gather more comprehensive data, including molecular force images, net cellular traction and force orientation.

As a proof of concept, we prepared a 30 kPa PA hydrogel with 17 pN RSDTPs and 40 nm fluorescent nanospheres functionalized on its surface to simultaneously measure molecular integrin force and cellular traction in living cells. Figure 1b shows time-lapse confocal images of the FAs, mTFM, TFM and bright field of mouse embryonic fibroblasts (MEFs), where the cell traction forces visualized by both mTFM and TFM are clearly located at the adhesion sites indicated by enhanced green fluorescent protein (eGFP)–paxillin. Furthermore, confocal *z*-stack images revealed both the mTFM signals and fluorescent nanospheres were tightly distributed around the surface without discernible background signal within the hydrogel (Fig. 1c). Specifically, the mechanical unfolding threshold of a given DNA-based tension probes is dependent only on the number of base pairs and force applied geometry, which should be independent with the rigidity of substrates (Extended Data Fig. 3) and insensitive to loading rates within a physiologically relevant range[20]. This ensures the reliability of the method. Using time-lapse imaging, we then studied the spatiotemporal dynamics of FAs, molecular force and net cellular traction during cell spreading on hydrogels. The temporal evolution plots of mTFM and TFM intensities shown in Fig. 1d revealed that both mTFM and TFM intensities coordinated with FAs, implying that the total intensity of mTFM could also be a reliable indicator of the temporal variation in net cellular traction. In addition, mTFM on hydrogels has substantially higher spatial resolution than conventional TFM images as shown in Fig. 1e, and the magnified image shows that the resolution of the mTFM image on the hydrogel is similar to that on a coverslip and approaching the optical diffraction limit (zoom in Fig. 1b). Additionally, TFM also provided traction force vector data, which indicated that the force was directed to the cell center. If we treated MEFs with actin polymerization inhibitor cytochalasin D, the mTFM and TFM signals decreased virtually simultaneously as expected (Extended Data Fig. 4 and Supplementary Video 1). Importantly, this approach allows us to continuously record mTFM, TFM and so on of cells for more than 7 h (Supplementary Video 2).

Furthermore, given that cellular traction may cause a local aggregation of DNA probes on soft hydrogel surfaces, we sought to determine if the unavoidable aggregation of folded DNA tension probes would result in a false signal. Specifically, we functionalized the hydrogel

Fig. 1 | Molecular tension probes coupled with TFM to jointly report cell adhesion force on hydrogel substrate. a, Schematic of the development of hydrogel-based mTFM method. Top left: molecular tension probe is preattached to Au NPs. Bottom left: schematic of cells spreading on a hydrogel substrate functioned with both molecular tension probes and fluorescent nanobeads. Middle: schematic of imaging cell molecular tensions and net tractions using fluorescent nanobeads and tension probes, respectively. Right: attachment of molecular tension probe to the hydrogel substrate. **b**–**d**, Representative time-lapse confocal imaging of eGFP–paxillin, mTFM, TFM and bright field (BF) of MEF cells on 30 kPa hydrogel substrate (**b**) and their corresponding plot as a function of time ($n = 4$ cells) (**d**), and representative 3D distribution of fluorescent signals collected from eGFP–paxillin of MEF cells, 17 pN RSDTPs and fluorescent nanobeads on 30 kPa hydrogel substrate (**c**). In **b** and **d**, data represent mean ± s.d. from three independent experiments. In **c**, the images are representative of two independent experimental results. **e**, Intensity profiles of paxillin, tension signals and net tractions along the white line marked in **b**. **f**, Representative confocal imaging of eGFP–LifeAct, mTFM and TFM of THP-1–M2 cells on 30 kPa hydrogel substrate. The images are representative of three independent experimental results. **g**,**h**, Intensity profiles of actin, tension signals and net tractions along the marked lines in zoom 1 (**g**) and zoom 2 (**h**) of **f**, respectively.

https://doi.org/10.1038/s41592-023-02037-0

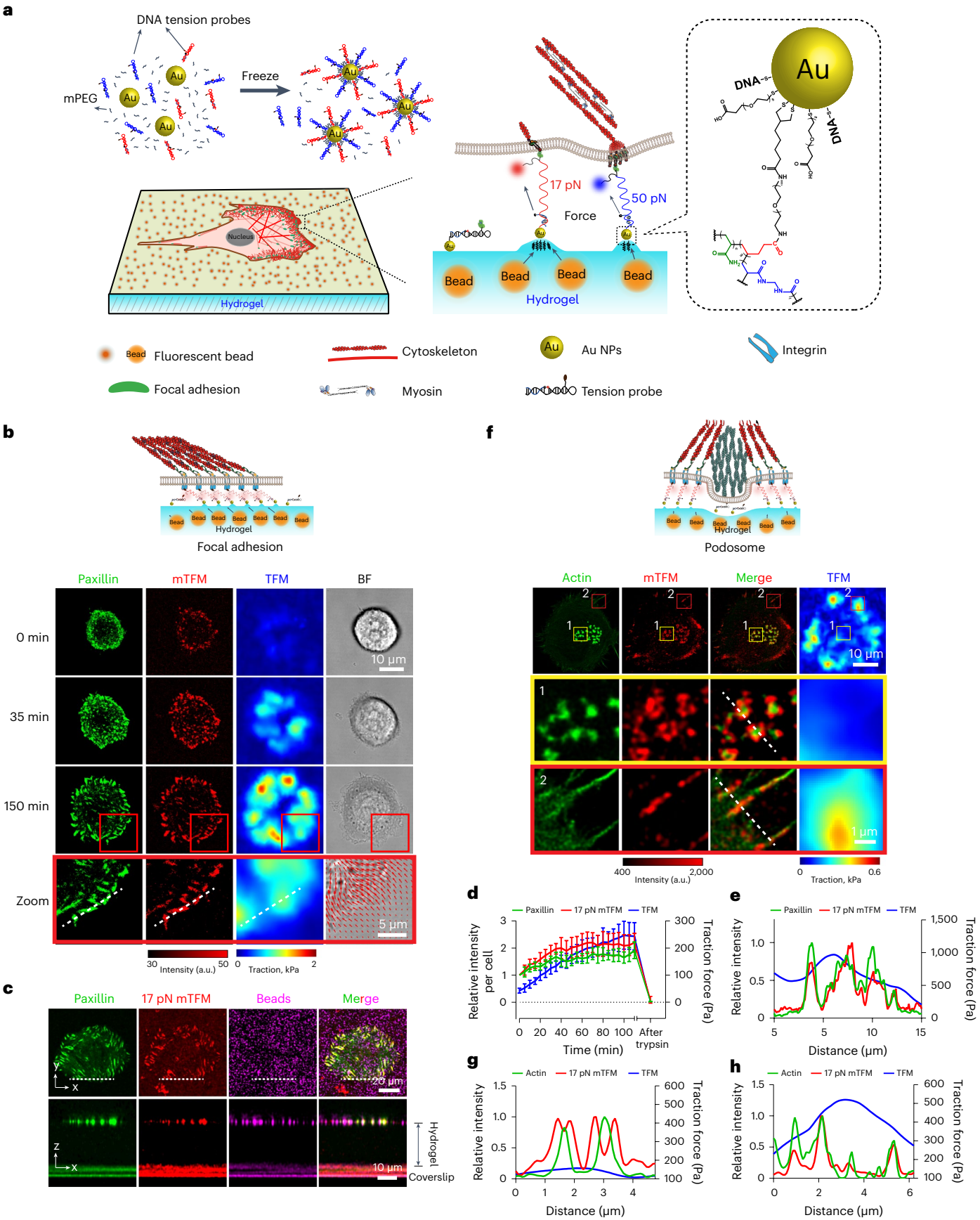

surface with scrambled DNA probes that do not unfold under cellular force but have a quenching efficiency similar to that of a regular folded DNA tension probe[15] (Extended Data Fig. 5a). As a result, cells could adhere properly to the modified hydrogels (Extended Data Fig. 5b), but we did not observe a substantial increase of background signals in FA areas where the scrambled DNA probes should have clustered under force similar to that of RSDTPs (Extended Data Fig. 5c). These results further confirmed the reliability of the mTFM signal measured on hydrogel surfaces.

Podosomes are specialized adhesion structures abundant in macrophages with actin-rich cores surrounded by integrin-rich rings less than a few microns in diameter[21], and their integrin-mediated adhesive forces have been shown to be small and nearly perpendicular to the substrate[22], beyond the capability of conventional TFM. Thus, we wondered whether the integrin forces of podosomes on hydrogels could be mapped using mTFM. We seeded macrophages transfected with eGFP–LifeAct on hydrogels prepared according to the above method for 1 h and found that both fibrillar FAs and columnar podosomes were formed (Fig. 1f–h). Forces at FAs were recorded by TFM at a lower spatial resolution than those of mTFM, similar to the above MEF cell results (zoom 2 in Fig. 1f,h). Interestingly, we found that the small ring-like integrin forces of podosome structures that were not visible on the TFM image were clearly visualized on the mTFM image (zoom 1 in Fig. 1f,g), with features consistent with previous reports[22,23]. Overlay and time-lapse images of mTFM and actin immunofluorescence images show that the integrin-mediated forces are always tightly surround the actin core (Supplementary Video 3).

Altogether, these results clearly demonstrate that the proposed procedure of mTFM can measure molecular forces in living cells on hydrogels; furthermore, the method could be combined with and complemented by the conventional TFM technique to visualize the cell tractions at subcellular and molecular scale simultaneously.

Quantifying molecular forces in cellular rigidity sensing

Given that we can measure molecular forces on hydrogels using mTFM, we wanted to determine how cells respond to ECM rigidity via integrin-mediated molecular forces. We prepared a series of hydrogels with different moduli ranging from 1 kPa to 80 kPa and functionalized their surface with multiplexed RSDTPs (17 pN and 50 pN RSDTPs were mixed at a 1:1 molar ratio) to simultaneously report total force-bearing integrins (>17 pN) and mechanically strongly loaded integrins (>50 pN) within the same cell (Fig. 2a, top). We adjusted the density of tension probes by fine-tuning the concentration and incubation time of Au NPs and RSDTPs, ensuring similar densities on hydrogels (~1,600 DNA probes μm^{-2}) with various stiffness (Methods and Supplementary Fig. 3), thereby eliminating the effects of density on force–stiffness characteristics. Note that the critical force for RSDTPs[15] or tension gauge tethers (TGTs)[24] is dependent on the force loading rate and observation time scale[25]. Therefore, the RSDTPs or TGTs with varying tension values utilized in our study represent differences in the mechanical stability of the DNA probes, rather than the precise force values exceeded by integrins during the experiments. In addition, we also measured the net traction force of cells on the different hydrogels using TFM (Fig. 2a, bottom). The results showed that both the size of FAs and the area of cell spreading increased as the DNA tension probe-functionalized hydrogels became stiffer, indicating that DNA tension probes do not interfere with the rigidity sensing process of MEFs (Fig. 2b). Moreover, the intensity of mTFM images with 17 pN RSDTPs shared a similar trend with that of TFM images (Supplementary Fig. 5), indicating that the number of integrins with tensions higher than 17 pN also increased as a response to increasing stiffness (Fig. 2c).

We noted that the mTFM images reported by 17 pN and 50 pN probes are both clearly distinguishable from the background. By calculating the total fluorescence intensity of both tension probes for each cell and correcting the fluorescence efficiency differences between the two channels, we found, surprisingly, that percentages of strongly loaded integrins (>50 pN) in the total force-bearing integrins (>17 pN) in cells remained at approximately 45% (Fig. 2d), even after the substrate modulus increased by more than an order of magnitude and the net cellular tractions increased by more than four-fold (Fig. 2e). Notably, this independence of integrin force distribution from substrate stiffness was also observed in other cell lines, including mouse myoblast cells (C2C12), human osteosarcoma cells (U2OS), Chinese hamster ovary cells (CHO), human glioblastoma cells (U251) and human cervical cancer cells (HeLa), and the slight difference in force ratio values between these cell lines was also successfully detected (Extended Data Fig. 6). This result suggested that the average magnitude of integrin forces in these cells is insensitive to ECM stiffness, which seems counterintuitive. Because it is commonly expected that if the net traction reported by TFM decreases as the ECM softens, the average magnitude of single integrin forces in FAs should decrease as well[8]. It is worth noting that all our experimental results were observed in the presence of serum, while the growth factor EGFR has been reported by Rao et al. to tune the mechanical tension threshold for outside-in integrin activation, cell spreading and FA maturation processes[26].

Note that, despite the reduction in mechanical stability of DNA probes when the ambient temperature increases to 37 °C (ref. 25), the mechanical stability difference between 17 pN RSDTPs and 50 pN RSDTPs remains notable (Extended Data Fig. 7). Furthermore, the magnitudes of integrin forces of cells adhering to various hydrogel surfaces were also challenged by 55 pN TGTs at room temperature (Fig. 2f), and the results showed that while alterations in ECM stiffness can substantially influence the spreading area and FA size of cells, the mechanical strength of integrin molecules within these cell adhesions is not substantially affected.

Moreover, we specifically knocked out vinculin using CRISPR/Cas9 (Vcl-KO), which disrupted the nuclear translocation of YAP without affecting the formation of FAs (Supplementary Fig. 6), and then compared the FA area, net tractions, and integrin tensions of Vcl-KO MEFs to those of wild-type MEFs using the same procedure described above (Fig. 2g). While Vcl-KO MEFs were still able to sense and respond to stiffness by regulating the size of the FAs (Fig. 2h), mTFM results showed that integrins carrying large forces (>50 pN) were substantially inhibited (Fig. 2g,i and Extended Data Fig. 8) by knockout of vinculin, consistent with the recent findings of Austin et al.[27], and this appears to be the main reason for the decrease in net traction of Vcl-KO MEFs (Fig. 2j). Furthermore, the magnitude of molecular force of integrins in FA did not increase no matter the Vcl-KO MEFs were spreading on soft, stiffer hydrogel substrate, or even on glass (Extended Data Fig. 8).

Taken together, our results indicated that cells respond to substrate rigidity, at least between 1 kPa and 80 kPa, probably in a 'digital' manner. As substrate stiffness increases, cells would recruit more integrins into FAs to carry part of the increased mechanical loading, rather than by increasing the mechanical strength of the existing integrin–ligand bonds, to facilitate FA maturation.

Exploring impact of hydrogel stiffness on integrin dynamics

Although prior investigations and theories have indicated that cells may respond to ECM stiffness via integrin–ECM binding dynamics[8,9], there is no experimental approach to directly examine this concept. Ma et al. recently developed a technique that utilizes locked oligonucleotides to irreversibly bind mechanically stretched DNA probes, therefore locking up the short-lived TCR-mediated forces and storing them in an mTFM history map[28]. Inspired by this idea, we attempt to extend the application of this method for probing receptor–ligand binding dynamics on different hydrogel substrates. Specifically, we designed a 29 nt single-stranded DNA molecule, called the locking strand, that can selectively hybridize to the mechanically unfolded RSDTPs on the

https://doi.org/10.1038/s41592-023-02037-0

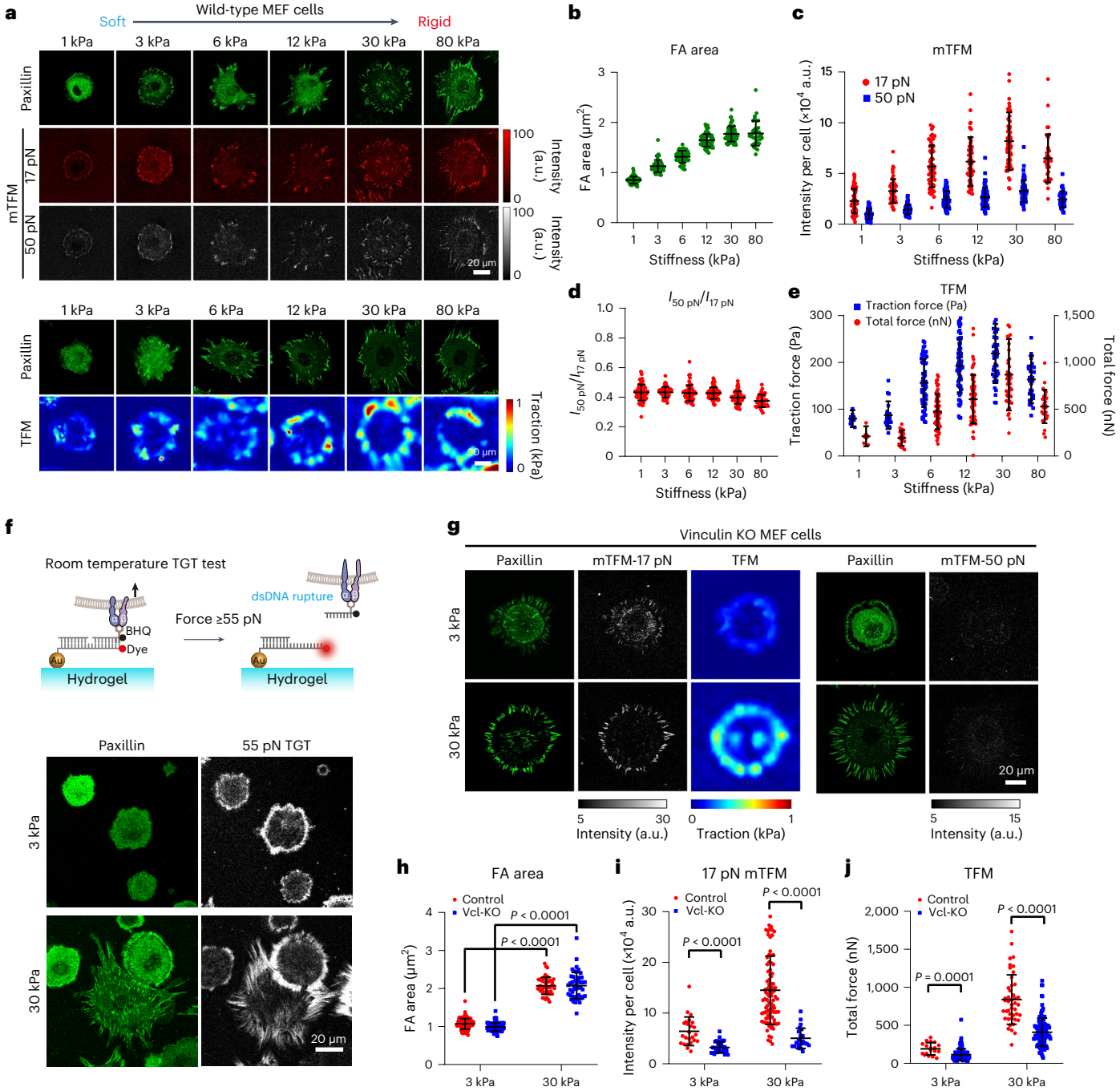

Fig. 2 | Probing the integrin-mediated molecular forces and net tractions of FAs during rigidity sensing. a, Representative fluorescent images of paxillin-tagged MEFs on multiple hydrogel substrates with rigidities ranging from 1 kPa to 80 kPa, and corresponding mTFM simultaneously reported by mixed 17 pN RSDTPs and 50 pN RSDTPs (top), and representative TFM results of cells seeded on hydrogels co-modified with fluorescent nanobeads and 17 pN RSDTPs (bottom). The images are representative of three independent experimental results. **b**–**e**, Plots of FA area (**b**), molecular tensions (**c**), ratio of strongly loaded integrin to total loaded integrins ($n = 64, 54, 59, 69, 62, 35$ cells for each stiffness) (**d**), and net traction of MEFs ($n = 4, 18, 59, 62, 44, 26$ cells for each stiffness) as a function of hydrogel stiffness (**e**). Data are mean ± s.d. from three independent experiments. **f**, Top: schematic of the measurement of integrin force on the hydrogel surface using TGTs labeled with a Cy3B and a Black Hole Quencher (BHQ). Bottom: representative fluorescent images of paxillin-tagged MEFs on soft (3 kPa) and stiff (30 kPa) hydrogels, and corresponding signals of 55 pN TGTs at room temperature (22 °C). The images are representative of three independent experimental results. dsDNA, double-stranded DNA. **g**, Representative fluorescent images of paxillin-tagged Vcl-KO MEF cells on soft (3 kPa) and stiff (30 kPa) hydrogel substrates and corresponding TFM and mTFM results visualized either by 17 pN RSDTPs or 50 pN RSDTPs. The images are representative of three independent experimental results. **h**–**j**, Quantification of the effect of Vcl-KO on the mechanical responses of MEFs to substrate stiffness using FA area (control, $n = 131, 48$ cells for each stiffness; Vcl-KO, $n = 97, 46$ cells for each stiffness) (**h**), 17 pN tension signals (control, $n = 24, 92$ cells for each stiffness; Vcl-KO, $n = 31, 23$ cells for each stiffness) (**i**) and net tractions (control, $n = 18, 44$ cells for each stiffness; Vcl-KO, $n = 108, 121$ cells for each stiffness) (**j**). Data are mean ± s.d. from three independent experiments. Two-tailed Student's *t*-tests are used to assess statistical significance.

surface and prevent its refolding, even if the integrin–ligand link is subsequently ruptured (Fig. 3a). Thus, if the dynamics of integrin–ligand binding vary with substrate rigidity, we can quantify the dynamics of integrin–ligand interactions as the mechanical sampling rate of the force-bearing integrins (Fig. 3b), which is the increasing rate of the total mTFM intensity computed using time-lapse imaging of mTFM after the addition of the locking chain (Supplementary Fig. 7).

To demonstrate this strategy, we first seeded MEF cells on the hydrogels (3 kPa) for 3 h, and the time lapse of mTFM signals with and without locking strands was collected. Apparently, mTFM signals remained stable, displaying no notable change in fluorescence intensity in the absence of locking strands or after the addition of unpaired locking strands (Extended Data Fig. 9). In contrast, after the addition of locking strands, mTFM clearly recorded the traces of cellular tension variation, which persisted even after treating cells with Cytochalasin D at a later timepoint to eliminate cellular forces (Extended Data Fig. 10). Furthermore, the cumulative amount of mTFM signals increased progressively over time following the addition of the locking strand until the locking strand was exhausted, and their rates were clearly higher than that of background signals resulted from force-independent locking strands–RSDTPs competitive pairing in non-cellular regions (Supplementary Fig. 7). These observations demonstrated the functionality and specificity of the locking strands in this experiment.

Next, we sought to further investigate the effect of hydrogel stiffness on integrin–RGD binding dynamics by conducting the aforementioned experiments on different hydrogel surfaces. The results showed that the intensity of all mTFM images gradually increased over time after adding the locking strands, as expected (Fig. 3c). By subtracting the background and normalizing the mean intensity of the mTFM images at $t = 0$ (before adding the locking strand), we obtained a growth curve over time (Fig. 3d). Moreover, by calculating the slope of the curve's increase during the first 5 min as a mechanical sampling factor, which reflects the fold increase of the integrated mTFM signal and quantitatively describes the integrin binding dynamics, we determined a mechanical sampling factor for a cell in relation to the ECM stiffness. The results of these analyses clearly revealed the distinguished response of the integrin–RGD binding dynamics of cells to hydrogel stiffness (Fig. 3e). Specifically, on a soft hydrogel (1 kPa), the mTFM signal could rise four-fold in 5 min but only two-fold within the same period on an intermediate rigid hydrogel (6 kPa). Interestingly, the mTFM signal again increased substantially when cells spread on a stiffer hydrogel (80 kPa). Further, this biphasic relationship between mechanical sampling factor and matrix stiffness is more notable in the statistics diagram as illustrated in Fig. 3e, thus suggesting that the binding frequency between integrins and RGD molecules is faster when cells are spread on soft and stiff hydrogels versus intermediate stiffness hydrogels. A possible explanation for this observation is that on a soft surface, where fibroblasts fail to form stable adhesions, the cells may frequently test the surface by forming transient force-transmission linkages, resulting in a high mechanical sampling rate of cells. At intermediate stiffness (for example, 30 kPa), mature FAs containing numerous ECM-bound integrins form, connected to the cytoskeleton by crosslinked stress fibers, resulting in more stable integrin–ECM linkages and a lower mechanical sampling rate. On a stiffer substrate, the development of coarser stress fibers, larger FA size and reduced hydrogel deformability may contribute to an increased force loading rate for integrins within FAs, which is likely to ultimately reduce the stability of individual integrin–ECM linkage in FAs[9].

Interestingly, after further characterizing the mechanical sampling factors of human glioblastoma cancer cell (U251), which have recently been shown to exhibit negative durotaxis behavior[29], we found the biphasic relationship was clearly absent (Fig. 3f,g), and the mechanical sampling factors of U251 on soft hydrogels (~1–10 kPa) were much lower than those on rigid hydrogels (>30 kPa), which is distinguished from MEFs (Fig. 3h). Although we do not yet fully understand the underlying molecular mechanism causing these distinct stiffness-dependent mechanical sampling rates between MEF and U251 or their link to cell migration behavior, it is evident that integrin–ECM binding kinetics are more sensitive to substrate rigidity compared to the magnitude of integrin tension in these cells (Fig. 3e,h). Taken together, these results experimentally confirm that cells can sense and respond to ECM rigidity through integrin–ligand binding dynamics. And these stiffness-dependent integrin–ECM binding kinetics, along with stiffness-invariant integrin tension, probably orchestrate the intricate mechanical response of cells to hydrogel stiffness.

Stiffness regulates T cell activation by TCR-mediated force

T cells exhibit mechanical sensitivity[30,31], and their TCR on the cell membrane transmit pN forces to improve immune recognition[13]. Furthermore, T cells are extremely sensitive to the stiffness of the interacting surface, and a more rigid matrix can notably boost the T cell immune response[32,33]. Despite this, how T cells regulate the mechanical properties of TCR–ligand interactions at the molecular level in response to variations in matrix rigidity remains unclear.

To quantitatively examine the immune response changes during T cell rigidity sensing, we cultured mouse naïve CD8 T cells on rigid (30 kPa) and soft (1 kPa) hydrogels functionalized with anti-CD3 and anti-CD28 antibodies. Using Fluo-4 time-lapse imaging, we tracked intracellular Ca^{2+} concentration changes, an early immune indicator[13,30] (Fig. 4a,b). CD8 T cells on rigid substrates showed higher Ca^{2+} concentrations within 2 min compared to the cells on soft substrates (Fig. 4c). In addition, comparing the rigid and soft substrates, cell spreading area, phosphorylation of ZAP70 (Y319), and CD69 expression increased by 12%, 50.4% and 59.6%, respectively (Fig. 4d–g).

We sought to further investigate the impact of matrix stiffness on the mechanical properties of the TCR–anti-CD3 complex using hydrogel-based mTFM. Initially, we explored the differences in TCR tension signals by using 12 pN DNA hairpin probes after T cells adhered to soft and rigid hydrogels for 15 min at room temperature (Fig. 4h). Note that previous single-molecule experiment[30] as well as T cell mechanics studies using DNA hairpin probes[13] has shown that ~12 pN is a threshold force for effective TCR activation. mTFM imaging revealed that T cells on a rigid matrix exhibited a notable circular mechanical pattern at their edges (Fig. 4i), similar to that observed on glass[13,28]. In contrast, on the soft hydrogel, TCR force was substantially attenuated, displaying

Fig. 3 | Probing the integrin–ECM binding dynamics on different hydrogels. **a**, Schematic diagram illustrating the principle of integrin-mediated force information storage. **b**, Characterizing the mechanical sampling rate of the integrins to ECM using locking strands. **c**,**d**, Representative time-lapse confocal imaging of 50 pN RSDTPs signals of MEF cells on hydrogel substrate with different stiffness after adding locking strands (**c**) and corresponding plots of their normalized accumulative intensity as a function of time ($n = 13, 17, 19, 22, 22, 19$ cells for each stiffness) (**d**). Data represent mean ± s.e.m. from three independent experiments. **e**, Quantification of the relationship between substrate stiffness and mechanical sampling factors of MEFs at 5 min after the addition of locking strands ($n = 13, 17, 19, 22, 22, 19$ cells for each stiffness). Data represent mean ± s.d. from three independent experiments. **f**,**g**, Representative time-lapse confocal imaging of 50 pN RSDTPs signals of U251-MG cells on hydrogel substrate with different stiffness after adding locking strands (**f**) and corresponding plots of their normalized accumulative intensity as a function of time ($n = 5, 11, 8, 9, 8, 9$ cells for each stiffness) (**g**). Data represent mean ± s.e.m. from three independent experiments. **h**, Quantification of the relationship between substrate stiffness and mechanical sampling factors at 5 min after the addition of locking strands ($n = 5, 11, 8, 9, 8, 9$ cells for each stiffness). Data represent mean ± s.d. from three independent experiments.

https://doi.org/10.1038/s41592-023-02037-0

only minimal, discontinuous and dot-like signals at cell edge (Fig. 4j). It should be noted that conventional TFM has difficulty in detecting the mechanical forces of T cells on more rigid hydrogels due to the relatively weaker forces of T cells (Supplementary Fig. 8). Additionally, similar to Fig. 3, we used a 4.7 pN DNA hairpin probe to investigate how the stiffness of the interacting surface regulates the kinetics of TCR–anti-CD3 interactions (Fig. 4k,l). Remarkably, on a rigid hydrogel, we observed a rapid increase in locked TCR tension signals

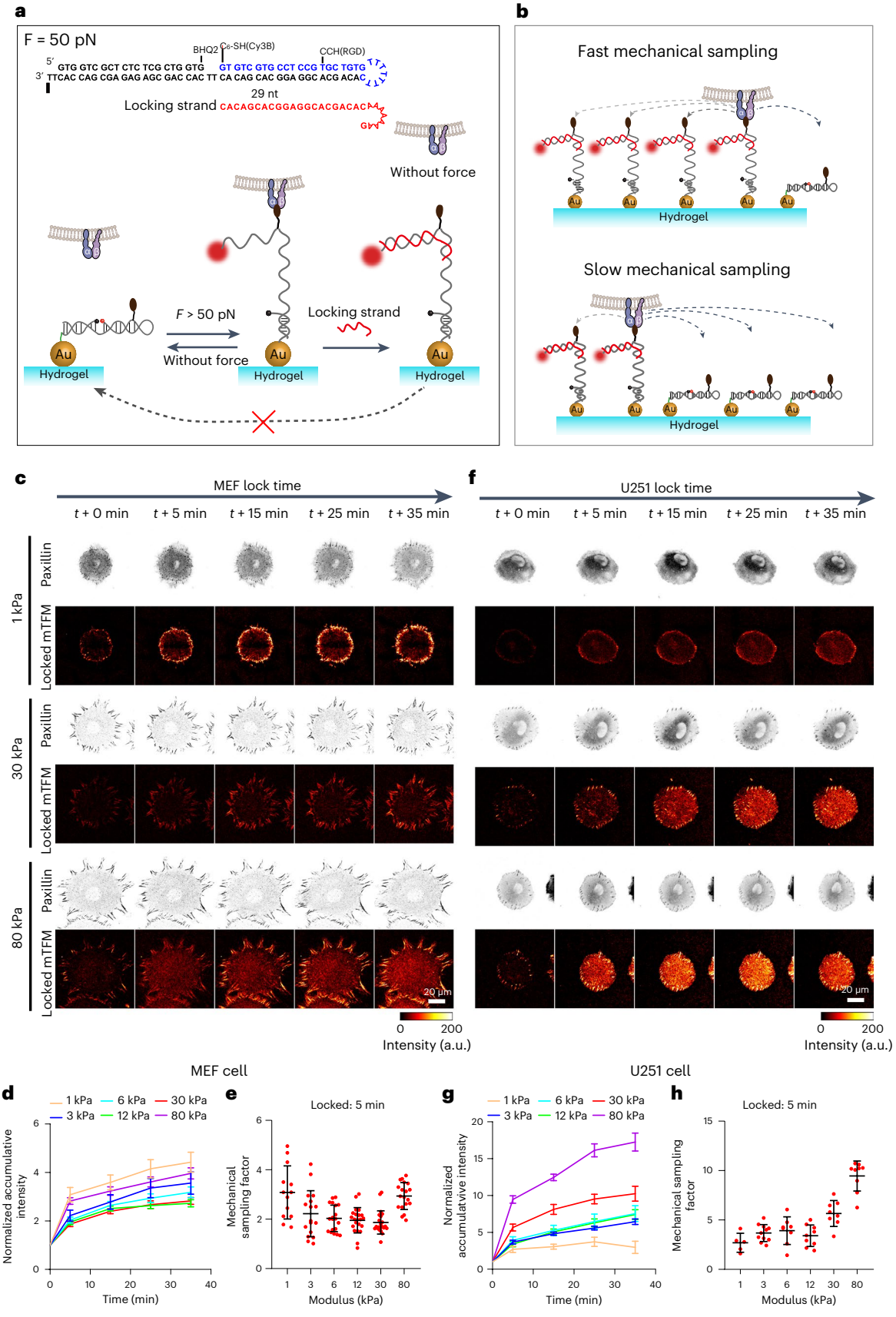

https://doi.org/10.1038/s41592-023-02037-0

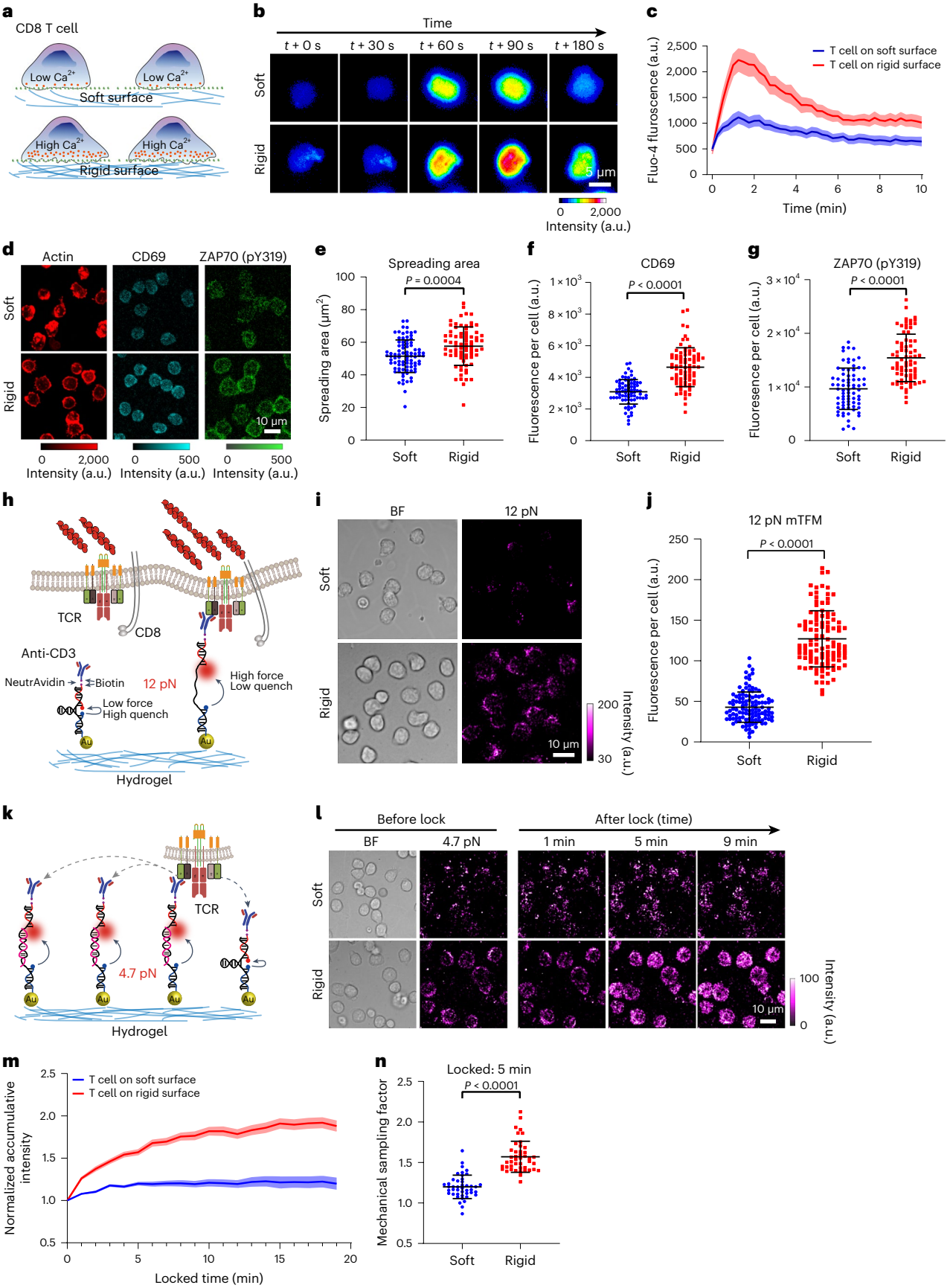

Fig. 4 | Stiffness-dependent activation of naïve T cells modulated by mechanical response of TCRs. a, Schematic diagram illustrating the response of intracellular Ca^{2+} concentration to substrate stiffness. **b**,**c**, Representative time-lapse fluorescent imaging of intracellular Ca^{2+} concentration of T cells seeded on soft (1 kPa) and rigid (30 kPa) hydrogels using Fluo-4 (**b**) and corresponding plots of their fluorescence intensity as a function of time (n = 21, 24 cells for each stiffness) (**c**). Data represent mean ± s.e.m. from three independent experiments. **d**–**g**, Representative immunofluorescence results of actin, CD69, and ZAP70 (pY319) of T cells after seeded on different hydrogel (**d**) and corresponding statistical comparison between their intensities on soft and rigid substrates (spreading area, n = 85, 76 cells for each stiffness (**e**); CD69, n = 78, 80 cells for each stiffness (**f**); ZAP70 (pY319), n = 75, 75 cells for each stiffness (**g**)). Data represent mean ± s.d. from three independent experiments. **h**, Schematic diagram illustrating the mechanism of hydrogel-based mTFM to report TCR–anti-CD3 interaction forces using 12 pN-hairpin. **i**,**j**, Representative bright field (BF) and mTFM images of T cells seeded on soft and rigid hydrogels (**i**) and corresponding total intensity per cell of mTFM signals (n = 115, 110 cells for each stiffness) (**j**). Data represent mean ± s.d. from three independent experiments. **k**, Schematic diagram illustrating the mechanism of locking strands in recording traces of TCR–anti-CD3 bonds. **l**,**m**, Representative time-lapse confocal imaging of 4.7 pN-hairpin signals of T cells on soft and rigid hydrogel after adding locking strands (**l**) and corresponding plots of their normalized accumulative intensity as a function of time (n = 44, 44 cells for each stiffness) (**m**). Data represent mean ± s.e.m. from three independent experiments. **n**, Quantification of the relationship between substrate stiffness and mechanical sampling factors of T cells at 5 min after the addition of locking strands (n = 44, 44 cells for each stiffness). Data represent mean ± s.d. from three independent experiments. Two-tailed Student's t-tests are used to assess statistical significance.

before reaching a plateau in approximately 10 min, similar to that observed on glass[28], which markedly differed from the slow and subtle changes in mTFM on soft hydrogels (Fig. 4m and Supplementary Videos 4 and 5). The statistical analysis of mechanical sampling factors further confirmed these differences in the temporal characteristics of TCR–anti-CD3 interactions (Fig. 4n).

These findings indicate that, when interacting with a soft antigen-presenting cell (APC), T cells face challenges in applying forces above the 12 pN threshold required to induce TCR conformational changes. Increased rigidity of the APC not only increases the force of TCR–ligand interactions, but also raises the mechanical scanning rate of T cells using the TCR against APC antigens, which ultimately improves the efficiency and precision of T cell recognition and activation.

Discussion

The invention of mTFM based on immobilized molecular tension probes has generated increasing interest in the field of mechanobiology because of its ability to visualize the mechanical force in living cells at the molecular level[16,34]. Unfortunately, mapping the cellular forces using mTFM on hydrogel surfaces that are closer to the Young's modulus of tissues has been challenging. To address this shortcoming, we present a general approach to specifically functionalize the hydrogel surface rather than the entire hydrogel matrix with tension probes by introducing Au NPs as specific docking sites on the hydrogel surface, thus enabling us to map the molecular force of living cells on hydrogels using mTFM. In addition, the developed method can be coupled with the conventional TFM method to provide more comprehensive information such as molecular force information, net cell traction and force orientation.

Hydrogel-based mTFM reveals an unexpected 'digital' response of integrin tension in adhesion sites to substrate stiffness, maintaining a nearly stable distribution of integrin force magnitude even when substrates stiffen more than ten-fold. We suspect that this digital behavior represents a conserved strategy allowing cells to recognize and respond to a wide range of stiffness without frequently fine-tuning the mechanical strength of existing integrin–ligand bonds to accommodate changing mechanical loads. Furthermore, by employing a locking strand reaction to quantify the dynamic characteristics of integrin–ECM interactions at the molecular level, we discovered that the sampling frequency of loaded integrins is more mechanosensitive to matrix stiffness than integrin tension distribution. This could be an effective strategy for cells to navigate in mechanically complex microenvironments. For instance, by accelerating the sampling frequency of force-bearing integrins on overly soft or stiff substrates, cells can rapidly explore the microenvironment until settling on substrates with favorable stiffness, at which point the sampling frequency can be downregulated. Notably, the importance of integrin–ECM kinetics in rigidity sensing suggested by our results is consistent with previous studies[6,29] that suggested the governing role of integrin–ligand dynamics in modulating durotaxis. These findings may offer a new perspective for exploring the relationship between the deconstruction of mechanosensory modules and the loss of rigidity sensing in tumor cells during transformed growth[35].

Moreover, hydrogel-based mTFM reveals that ECM rigidity positively modulates both the pN force and frequency of TCR–ligand interactions, ultimately enhancing T cell activation. These findings not only demonstrate the potential of the hydrogel-based mTFM in examining the molecular forces of T cell rigidity sensing but also offer a unique perspective to interpret the stiffness as a mechanical checkpoint for T cell activation[36–38]. For instance, by increasing the number of >12 pN force activated TCRs and the 'trial and error' frequency during T cell activation, T cells could rapidly complete the screening of potential antigens presented by stiffening cancer cells as well as initiate the following up activation and killing if necessary. In contrast, when interacted with softer cancer cells, T cells are more likely to miss positive targets due to the weaker forces exerted on the TCR–ligand and the reduced efficiency of antigen screening, leading to possible immune escape and hampered T-cell-mediated cancer-cell killing in immunotherapy.

It should be noted that the reliance of hydrogel-based mTFM on a conventional confocal microscope for imaging presents potential challenges. Compared to the total internal reflection fluorescence (TIRF) microscopy typically used for mTFM experiments on coverslips, the signal-to-noise ratio of the confocal system is inferior, potentially compromising the precision of single-molecule images. In addition, our method, which was primarily developed for two-dimensional (2D) hydrogel interfaces, does not adapt seamlessly to three-dimensional (3D) hydrogels. Establishing robust techniques for measuring molecular mechanics in a 3D environment is a key direction for future efforts in this field.

Altogether, our results firmly demonstrated that the hydrogel-based mTFM method can enable the real-time imaging of the molecular forces as well as their dynamics in living cells on 2D hydrogels. Thus, we believe that this method will provide a powerful tool to reveal the molecular mechanisms underlying life processes involved in ECM stiffness-regulated mechanotransduction, such as rigidity sensing[39], durotaxis[29,40], immune cell–ECM interactions[36] and stem cell differentiation[1].

Online content

Any methods, additional references, Nature Portfolio reporting summaries, source data, extended data, supplementary information, acknowledgements, peer review information; details of author contributions and competing interests; and statements of data and code availability are available at https://doi.org/10.1038/s41592-023-02037-0.

References

1. Engler, A. J., Sen, S., Sweeney, H. L. & Discher, D. E. Matrix elasticity directs stem cell lineage specification. *Cell* **126**, 677–689 (2006).

2. Qiu, Y. Z. et al. Platelet mechanosensing of substrate stiffness during clot formation mediates adhesion, spreading, and activation. *Proc. Natl Acad. Sci. USA* **111**, 14430–14435 (2014).
3. Levental, K. R. et al. Matrix crosslinking forces tumor progression by enhancing integrin signaling. *Cell* **139**, 891–906 (2009).
4. Polacheck, W. J. & Chen, C. S. Measuring cell-generated forces: a guide to the available tools. *Nat. Methods* **13**, 415–423 (2016).
5. Prager-Khoutorsky, M. et al. Fibroblast polarization is a matrix-rigidity-dependent process controlled by focal adhesion mechanosensing. *Nat. Cell Biol.* **13**, 1457–1465 (2011).
6. Plotnikov, S. V., Pasapera, A. M., Sabass, B. & Waterman, C. M. Force fluctuations within focal adhesions mediate ECM-rigidity sensing to guide directed cell migration. *Cell* **151**, 1513–1527 (2012).
7. Elosegui-Artola, A. et al. Mechanical regulation of a molecular clutch defines force transmission and transduction in response to matrix rigidity. *Nat. Cell Biol.* **18**, 540–548 (2016).
8. Elosegui-Artola, A., Trepat, X. & Roca-Cusachs, P. Control of mechanotransduction by molecular clutch dynamics. *Trends Cell Biol.* **28**, 356–367 (2018).
9. Elosegui-Artola, A. et al. Rigidity sensing and adaptation through regulation of integrin types. *Nat. Mater.* **13**, 631–637 (2014).
10. Stabley, D. R., Jurchenko, C., Marshall, S. S. & Salaita, K. S. Visualizing mechanical tension across membrane receptors with a fluorescent sensor. *Nat. Methods* **9**, 64–67 (2011).
11. Blakely, B. L. et al. A DNA-based molecular probe for optically reporting cellular traction forces. *Nat. Methods* **11**, 1229–1232 (2014).
12. Zhang, Y., Ge, C., Zhu, C. & Salaita, K. DNA-based digital tension probes reveal integrin forces during early cell adhesion. *Nat. Commun.* **5**, 5167 (2014).
13. Liu, Y. et al. DNA-based nanoparticle tension sensors reveal that T-cell receptors transmit defined pN forces to their antigens for enhanced fidelity. *Proc. Natl Acad. Sci. USA* **113**, 5610–5615 (2016).
14. Ma, V. P. Y. et al. The magnitude of LFA-1/ICAM-1 forces fine-tune TCR-triggered T cell activation. *Sci. Adv.* **8**, eabg4485 (2022).
15. Li, H. Y. et al. A reversible shearing DNA probe for visualizing mechanically strong receptors in living cells. *Nat. Cell Biol.* **23**, 642–651 (2021).
16. Blanchard, A. T. & Salaita, K. Emerging uses of DNA mechanical devices. *Science* **365**, 1080–1081 (2019).
17. Ma, V. P. Y. et al. Ratiometric tension probes for mapping receptor forces and clustering at intermembrane junctions. *Nano Lett.* **16**, 4552–4559 (2016).
18. Liu, Y., Yehl, K., Narui, Y. & Salaita, K. Tension sensing nanoparticles for mechano-imaging at the living/nonliving interface. *J. Am. Chem. Soc.* **135**, 5320–5323 (2013).
19. Liu, B. W. & Liu, J. W. Freezing-driven DNA adsorption on gold nanoparticles: tolerating extremely low salt concentration but requiring high DNA concentration. *Langmuir* **35**, 6476–6482 (2019).
20. Zhang, T. B. et al. Determination of base binding strength and base stacking interaction of DNA duplex using atomic force microscope. *Sci. Rep.* **5**, 9143 (2015).
21. van den Dries, K. et al. Modular actin nano-architecture enables podosome protrusion and mechanosensing. *Nat. Commun.* **10**, 5171 (2019).
22. Glazier, R. et al. DNA mechanotechnology reveals that integrin receptors apply pN forces in podosomes on fluid substrates. *Nat. Commun.* **10**, 4507 (2019).
23. Pal, K., Tu, Y. & Wang, X. Single-molecule force imaging reveals that podosome formation requires no extracellular integrin–ligand tensions or interactions. *ACS Nano* **16**, 2481–2493 (2022).
24. Wang, X. & Ha, T. Defining single molecular forces required to activate integrin and notch signaling. *Science* **340**, 991–994 (2013).
25. Liu, J. et al. Tension gauge tethers as tension threshold and duration sensors. *ACS Sens.* **8**, 704–711 (2023).
26. Rao, T. C. et al. EGFR activation attenuates the mechanical threshold for integrin tension and focal adhesion formation. *J. Cell Sci.* **133**, jcs238840 (2020).
27. Austin, J., Tu, Y., Pal, K. & Wang, X. F. Vinculin transmits high-level integrin tensions that are dispensable for focal adhesion formation. *Biophys. J.* **122**, 156–167 (2023).
28. Ma, R. et al. DNA probes that store mechanical information reveal transient piconewton forces applied by T cells. *Proc. Natl Acad. Sci. USA* **116**, 16949–16954 (2019).
29. Isomursu, A. et al. Directed cell migration towards softer environments. *Nat. Mater.* **21**, 1081–1090 (2022).
30. Liu, B. Y., Chen, W., Evavold, B. D. & Zhu, C. Accumulation of dynamic catch bonds between TCR and agonist peptide-MHC triggers T cell signaling. *Cell* **157**, 357–368 (2014).
31. Li, Y. C. et al. Cutting edge: mechanical forces acting on T cells immobilized via the TCR complex can trigger TCR signaling. *J. Immunol.* **184**, 5959–5963 (2010).
32. Saitakis, M. et al. Different TCR-induced T lymphocyte responses are potentiated by stiffness with variable sensitivity. *eLife* **6**, e23190 (2017).
33. Blumenthal, D., Chandra, V., Avery, L. & Burkhardt, J. K. Mouse T cell priming is enhanced by maturation-dependent stiffening of the dendritic cell cortex. *eLife* **9**, e55995 (2020).
34. Roca-Cusachs, P., Conte, V. & Trepat, X. Quantifying forces in cell biology. *Nat. Cell Biol.* **19**, 742–751 (2017).
35. Yang, B. et al. Stopping transformed cancer cell growth by rigidity sensing. *Nat. Mater.* **19**, 239–250 (2020).
36. Tello-Lafoz, M. et al. Cytotoxic lymphocytes target characteristic biophysical vulnerabilities in cancer. *Immunity* **54**, 1037–1054.e7 (2021).
37. Lei, K. et al. Cancer-cell stiffening via cholesterol depletion enhances adoptive T-cell immunotherapy. *Nat. Biomed. Eng.* **5**, 1411–1425 (2021).
38. Liu, Y. et al. Cell softness prevents cytolytic T-cell killing of tumor-repopulating cells. *Cancer Res.* **81**, 476–488 (2021).
39. Kechagia, J. Z., Ivaska, J. & Roca-Cusachs, P. Integrins as biomechanical sensors of the microenvironment. *Nat. Rev. Mol. Cell Biol.* **20**, 457–473 (2019).
40. Lo, C. M., Wang, H. B., Dembo, M. & Wang, Y. L. Cell movement is guided by the rigidity of the substrate. *Biophys. J.* **79**, 144–152 (2000).

Methods

Animals

C57BL/6-Tg (TcraTcrb)1100Mjb/J transgenic mice were housed and bred following the protocol approved by the Institutional Animal Care and Use Committee, ABSL-3 Laboratory Institutional Biosafety Committee of Wuhan University (Animal Using Protocol: WP2020-08127) after kindly provided by the laboratory of Prof. Yucai Wang (University of Science and Technology of China). Mice were maintained under specific pathogen-free conditions (20–25 °C temperature and 50–60% humidity), and there were five mice housed in each standard cage under 12 h-light and 12 h-dark cycles while fed ad libitum with a standard chow diet. Before splenocytes were isolated, mice were anesthetized with carbon dioxide and sacrificed for cervical dislocation. The experimental protocols of this study were designed according to the '3Rs' principle—replacement, reduction and refinement—and strictly in accordance with the Regulations on the Management of Laboratory Animals, the Guiding Opinions on the Ethical Treatment of Laboratory Animals of the Ministry of Science and Technology of China, the Regulations on the Management of Laboratory Animals of Hubei Province, and other relevant national laws and regulations. All mouse experiments were conducted in accordance with internationally accepted guidelines, and there was no abuse of laboratory animals or ethical violations.

Cell culture, transfection and constructs

THP-1 (SCSP-648), CHO (SCSP-507), MEF (SCSP-105), U2OS (SCSP-5030), U251-MG (TCHu 58), C2C12 (SCSP-505) and HeLa (SCSP-504) cells were purchased from Stem Cell Bank, Chinese Academy of Science. MEF, HeLa, U2OS and C2C12 cells were cultured in Dulbecco's modified Eagle Medium (Sangon Biotech, E600003-0500) supplemented with 10% fetal bovine serum (FBS, VivaCell, C04001-500), penicillin G (100 IU ml^{-1}, Sangon Biotech, E607011-0100) and streptomycin (100 μg ml^{-1}, Sangon Biotech, E607011-0100) and incubated at 37 °C with 5% CO_2. CHO cells were cultured in F-12K Medium (Kaighn's Modification of Ham's F-12 Medium, Gibco, 21127022), supplemented with 10% FBS and incubated at 37 °C with 5% CO_2. U251 cells were cultured in Dulbecco's modified Eagle medium/F-12 (Gibco, 11320-074) supplemented with 10% FBS, penicillin G (100 IU ml^{-1}) and streptomycin (100 μg ml^{-1}) and incubated at 37 °C with 5% CO_2.

THP-1 cells were cultured in Roswell Park Memorial Institute medium (RPMI-1640, Sangon Biotech, E600028-0500) supplemented with 10% FBS, penicillin G (100 IU ml^{-1}), streptomycin (100 μg ml^{-1}) and 0.55 mM 2-mercaptoethanol (Gibco, 21985023) at 37 °C with 5% CO_2. The suspended THP-1 monocyte cells were differentiated into adherent macrophage-like cells with 10 μg ml^{-1} phorbol 12-myristate 13-acetate (Sigma, P8139) for 48 h. Macrophage M2 polarization was obtained by incubation with 20 ng ml^{-1} of interleukin 4 (R&D Systems, 204-IL).

Naïve CD8 T cells were isolated from the splenocytes of C57BL/6-Tg (TcraTcrb)1100Mjb/J transgenic mice (6–8 weeks of age, both male and female) using Mouse CD8 T Cell Isolation Kit (BioLegend, 480008) following protocol provided by the manufacture. CD8 T cells were cultured in RPMI-1640 supplemented with 10% FBS, penicillin G (100 IU ml^{-1}) and streptomycin (100 μg ml^{-1}).

eGFP–LifeAct and eGFP–paxillin lentiviral expression plasmids were gifts from Prof. Congying Wu lab (Peking University, China). To knock out vinculin using CRISPR, the selected DNA sequences (target sequences 1: 5′-gctgacggccgcctgcacgg-3′, target sequences 2: 5′-gcacctggtgattatgcacg-3′) were designed and cloned into PX459-CPISPR/Cas 9 plasmid gifted by Prof. Kai Jiang lab (Wuhan University, China). All transfections were carried out using the Lipofectamine 3000 Transfection Reagent (Invitrogen, L3000015) following the manufacturer's instructions.

Synthesis of molecular tension probes and their calibration

The structures and modification of oligonucleotides that were used to synthesize RSDTPs, TGTs and hairpins were purchased from Sangon Biotech as detailed in Supplementary Fig. 1 and Supplementary Data. The synthesis of RSDTPs with different unfolding thresholds followed the procedures developed by the Liu lab previously[15]. Briefly, strand I was ligated with strand II using DNA ligase to obtain strand X, which was later hybridized with strand III to form RSDTPs as shown in Extended Data Fig. 1 (also see Supplementary Note). TGTs and hairpins with different rupture forces were designed on the basis of a previous report by the Ha lab[24] and the Salaita lab[13], respectively, but slightly adjusted to form Au NP–probe complexes as shown in Supplementary Fig. 1, and their synthesis is also illustrated in Extended Data Fig. 1. The anti-CD3 was attached to the free end of hairpins immobilized on hydrogels through the biotin–NeutrAvidin (Thermo Scientific, 31000) bond following the protocol detailed by Salaita lab[13]. The dependence of molecular tension probes on hydrogel stiffness was calibrated using magnetic tweezer following the reported protocol[15].

PA hydrogel preparation and characterization

The preparation of PA hydrogels with fluorescent nanobeads coated on the surfaces is illustrated in Extended Data Fig. 2a[41]. Briefly, 25 mm and 12 mm coverslips were firstly functionalized with aldehyde groups and fluorescent nanobeads, respectively. Then, 6 μl of PA hydrogel aqueous solution prepared as in Extended Data Fig. 2d was dropped on the modified 25 mm cover glass, which was quickly covered by the modified 12 mm cover glass with coated fluorescent nanobeads facing downwards. After the hydrogel solidified, the two coverslips were carefully separated to form a layer of PA hydrogel (about 20–30 μm thick) coated by the fluorescent nanobeads on the surface of 25 mm coverslips. To remove unpolymerized acrylamide in the hydrogel networks, the prepared hydrogels were rinsed twice before immersion in phosphate-buffered saline (PBS) at 4 °C for later use.

The Young's modulus of prepared hydrogels was characterized using AFM (BioScope Resolve, Bruker) and a silicon nitride AFM probe with a tip radius of 65 nm and a calibrated spring constant of $k = 0.089$ N m^{-1} (PFQNM-LC-A-CAL, Bruker). For each sample, ten force–displacement curves were recorded with a peak-to-peak amplitude of 5 μm and force amplitude of 400 pN at a frequency of 5 Hz. The Hertz model was then fitted to the retrace force–displacement curves to compute the modulus (Extended Data Fig. 2d,e).

Immobilization of DNA tension probes on hydrogel surfaces

Firstly, Au NPs of 13 nm were prepared following a standard protocol introduced by Haley et al.[42], and the concentration and Au NP size were determined using a NanoDrop microvolume spectrophotometer (Thermo Fisher) and high-resolution field emission transmission electron microscope (JEOL, JEM-2100, Supplementary Fig. 2a,b), respectively. Then, a 6.858 nM solution of citrate-stabilized Au NPs (13 nm) was incubated with 8.91 μM of COOH–PEG8–SH and 150 nM of Cy3B–RSDTPs (or a mixture of 100 nM Cy3B–RSDTPs and 100 nM 647N–RSDTPs) to form Au NP–DNA complexes (roughly four to five probes per Au NP as shown in Supplementary Fig. 3). Due to the existence of active carboxyl groups within hydrogel network introduced by the 4-pentenoic acid in the PA hydrogel aqueous solution, these complexes covalently attached to hydrogels network at similar density throughout the stiffness range studied in this paper (Supplementary Fig. 3). Specifically, hydrogels were incubated in 0.1 M MES buffer (pH 5.0) with 5 mM NH_2–PEG–lipoic acid (molecular weight of PEG ~1,000 g mol^{-1}) for 3 h at room temperature to introduce lipoic acid groups (Extended Data Fig. 2b), and Au NP–DNA complexes were frozen at −80 °C for 1 h before addition onto the hydrogel surface (Extended Data Fig. 2c). After incubation at room temperature for 30 min to allow the formation of covalent bond between Au NPs and hydrogels, the hydrogel was washed five times with PBS to remove unbound probes before cell seeding.

Characterization of density of RSDTPs on hydrogels

The density of RSDTPs functionalized on hydrogels was characterized by quantifying the number of probes per Au NPs using TIRF and the

density of Au NPs on hydrogels using field emission scanning electron microscopy (Zeiss, GeminiSEM 500). Specifically, to examine the dependence of number of probes per Au NPs on the concentration ratio of Au NPs to RSDTPs, we firstly synthesized unfolded probes mimicking the unfolded conformation of RSDTPs and mixed them with Au NPs and methoxy polyethylene glycol (mPEG) before freezing for 1 h (Supplementary Fig. 3a). After dilution to 1 nM, the mixture was incubated on the glass coverslip for 1 h. Next, we used single molecular photobleaching to identify the fluorescence intensity of a single unfolded probe, and the number of unfolded probes per Au NP was then determined from the fluorescence intensity of single unfolded probe–Au NP particle for a specific concentration. Thus, by varying the dye and concentration, the relationship between concentration of Au NP–unfolded probe mixture and number of unfolded probes per Au NP was calibrated to direct the tuning of experimental conditions in preparing substrates with multiplexed probes (Supplementary Fig. 3b). Specifically, to ensure the number of 17 pN-Cy3B and 56 pN-647N on Au NP were similar, we mixed the Au NP, Cy3B unfolded probes and 647N unfolded probes at 1:15:15 concentration ratio based on the calibration curve, and the single molecular photobleaching results confirmed that there was approximately four Cy3B unfolded probes and four 647N unfolded probes attached to each Au NP on average (Supplementary Fig. 3d). Moreover, after dilution to 5 nM, the mixture was incubated on hydrogels, and the densities of the Au NPs immobilized on the surface of hydrogels at different stiffness were calibrated to be approximately 400 μm^{-2} under scanning electron microscopy (Supplementary Fig. 3c). Thus, the densities of both the 17 pN and 50 pN RSDTPs were determined to be ~1,600 μm^{-2} across conditions.

Western blots

Cells in culture were rinsed once with PBS and lysed directly in 4 °C RIPA buffer with protease inhibitor (Roche). After protein concentration was quantified using bicinchoninic acid kit (Sangon Biotech), loading buffer was added to cell lysates before incubation at 95 °C for 5 min and samples were run on 4–20% precast PA sodium dodecyl sulfate–polyacrylamide gel electrophoresis gels (Monad) in running buffer. Proteins were then transferred to polyvinylidene fluoride membrane (Sangon Biotech) using Wet Tank blotting system (Bio-Rad). The membrane was blocked with 5% dry milk–TBST for 1 h and incubated with GAPDH loading control monoclonal antibody (1:1,000, Thermo, MA5-15738) and primary antibody, that is, recombinant rabbit monoclonal antibody to vinculin (1:3,000, Thermo Fisher, 700062), at 4 °C overnight. The membrane was then washed thoroughly with TBST and incubated for 1 h at room temperature with horseradish peroxidase (HRP)-labeled secondary antibody including HRP-conjugated Goat Anti-Mouse IgG (1:5,000, Sangon Biotech, D110087) and HRP-conjugated Goat Anti-Rabbit IgG (1:5,000, Sangon Biotech, D110058), which were detected with ECL western blotting detecting reagents (Beyotime) on Gel Doc XR+ System (Bio-Rad) as shown in Extended Data Fig. 6d and quantified with ImageJ 1.53t.

Immobilization of antibodies on hydrogel surfaces

Firstly, PA hydrogels were prepared following the steps detailed in Extended Data Fig. 2d. Then, 300 µl 0.2 mg ml^{-1} Sulfo-SANPAH (Thermo Scientific, 22589) was added to the prepared PA hydrogel before exposure to UV light for 15 min. After the hydrogel was washed three times with PBS to remove free Sulfo-SANPAH, 30 µl 100 µg ml^{-1} NeutrAvidin (Thermo Scientific, 31000) was incubated with the Sulfo-SANPAH modified hydrogel overnight at 4 °C before free NeutrAvidin was removed. Next, the mixture of 50 µg ml^{-1} Biotin anti-mouse CD3ε Antibody (BioLegend, 100304) and 10 µg ml^{-1} Biotin anti-mouse CD28 Antibody (BioLegend, 102103) was added to NeutrAvidin modified hydrogel for 1 h at room temperature. Finally, the hydrogel was washed three times with PBS to remove unbound antibodies before seeding cells.

Fluorescence immunostaining

After seeded on hydrogels commodified with anti-CD3 and anti-CD28 at 37 °C, Naïve T cells were fixed with 4% paraformaldehyde at room temperature for 15 min and permeabilized with methanol anhydrous for 10 min at 4 °C before rinsing three times in PBS. Fixed cells were then blocked using 3% bovine serum albumin for 1 h at room temperature and washed three times in PBS. To label F-actin, the prepared samples were incubated with 1 µg ml^{-1} phalloidin-TRITC (Solarbio) for 1 h at room temperature (T cells were seeded for 30 min before fixing). A 1:50 dilution of mouse monoclonal FITC anti-mouse CD69 antibody (BioLegend, 104505) was used for immunostaining of CD69 expressing following the protocol provided by the manufacturer (T cells were seeded for 120 min before fixing). A 1:20 dilution of mouse monoclonal Alexa Fluor 647 anti-ZAP70 Phospho (Tyr319)/Syk Phospho (Tyr352) antibody (BioLegend, 683705) was used for immunostaining of phosphorylation of ZAP70 following the protocol provided by the manufacture (T cells were seeded for 45 min before fixing). For immunostaining of YAP in WT MEFs and Vcl-KO MEFs, a 1:200 dilution of mouse monoclonal anti-YAP (Santa Cruz Biotechnology, sc-101199) and a 1:200 dilution of Alexa Fluor 647-conjugated goat anti-mouse IgG (Sangon Biotech, D110109-0100) were used as primary and secondary antibodies following the protocol provided by the manufacturer, respectively. Finally, all the stained specimens were rinsed extensively with PBS, before microscopic observations.

Intracellular calcium imaging

Firstly, naïve T cells were labeled with Fluo-4 AM (Beyotime, S1060) following the protocol provided by the manufacture. Next, the labeled T cells were seeded on hydrogels commodified with anti-CD3 and anti-CD28, and the signals of calcium labels were recorded using time-lapse fluorescence microscopy for a duration of 25 min at 15 s intervals.

Traction force measurements

After cells were seeded for 3 h, fluorescent images of the coated nanobeads were captured both before and after trypsinization using a confocal microscope with a 63× oil objective to compute the deformation of the hydrogels generated by seeded cells. The cellular tractions were then calculated from the deformation map using the L2-based-FTTC methods developed by the Danuser lab[43] (The University of Texas Southwestern Medical Center, Texas, USA[44]).

Image acquisition and analysis

Both confocal microscope and TIRF microscope were adopted in this work. Specifically, cells seeded on hydrogels were imaged using a Leica TCS SP8/Zeiss LSM 880/Olympus FV3000 confocal microscope equipped with a 63× oil objective (numerical aperture 1.40) and microscope incubator (37 °C, 5% CO_2), while a Nikon Eclipse Ti2 TIRF microscope with an Apo TIRF 100× oil objective lens (numerical aperture 1.49) and an ANDOR EMCCD (1,024 × 1,024 pixels) camera were only used to characterize Au NP–DNA complexes on coverslips and quantify integrin tension of Vcl-KO MEF cells seeded on coverslips. The acquired tension images were processed with ImageJ 1.53t and MATLAB R2019a. Specifically, a three-step procedure including (1) background removal, (2) creation of a FA mask from eGFP–paxillin image and (3) application of the FA mask to the tension image was adopted for the calculation of integrin tensions at cellular and subcellular scales as shown in Supplementary Fig. 5a. Furthermore, FA masks were also used to analyze the response of cells to substrate stiffness including FA areas and spreading areas.

Statistical analysis

All statistical data were computed from three independent experiments using Excel 2019, Origin 9.0, GraphPad Prism 8.3.0 or MATLAB R2019a. The statistical significance between two cases were determined using

two-tailed Student's *t*-tests. The plotting and presentation of the results were completed in GraphPad Prism 8.3.0, Origin 9.0 or MATLAB R2019a.

Reporting summary

Further information on research design is available in the Nature Portfolio Reporting Summary linked to this article.

Data availability

All imaging data have been uploaded on Figshare (https://doi.org/10.6084/m9.figshare.24008127). Source data are provided with this paper.

References

41. Colin-York, H., Eggeling, C. & Fritzsche, M. Dissection of mechanical force in living cells by super-resolved traction force microscopy. *Nat. Protoc.* **12**, 783–796 (2017).
42. Hill, H. D. & Mirkin, C. A. The bio-barcode assay for the detection of protein and nucleic acid targets using DTT-induced ligand exchange. *Nat. Protoc.* **1**, 324–336 (2006).
43. Han, S. J., Oak, Y., Groisman, A. & Danuser, G. Traction microscopy to identify force modulation in subresolution adhesions. *Nat. Methods* **12**, 653–656 (2015).
44. Han, S. J., Oak, Y., Groisman, A. & Danuser, G. TFM. *GitHub* https://github.com/DanuserLab/TFM (2015).

Acknowledgements

This work was supported by the National Natural Science Foundation of China (32150016, 21775115, 32071305 and 31871356), the Fundamental Research Funds for the Central Universities (2042021kf0030) and Innovation Funds for Postdocs in Hubei Province.

Author contributions

Z.L. conceived the project and supervised the research. W.W. and W.C., with the help of P.L., H.L., J.F. and F.S., designed and performed the hydrogel-based mTFM and TFM coupling experiments and analyzed the data. W.W., C.W. and Y.H. designed and performed the T cell and podosome experiments. C.Z. and X.Z. performed single-molecule magnetic tweezer experiments, and K.J. provided intellectual input for the cell knockout experiments. Z.L., W.W. and W.C. wrote the paper with the help of others.

Competing interests

The authors declare no competing interests.

Additional information

Extended data is available for this paper at https://doi.org/10.1038/s41592-023-02037-0.

Supplementary information The online version contains supplementary material available at https://doi.org/10.1038/s41592-023-02037-0.

Correspondence and requests for materials should be addressed to Zheng Liu.

Peer review information *Nature Methods* thanks Sanjeevi Sivasankar, Tejeshwar Rao and the other, anonymous, reviewer(s) for their contribution to the peer review of this work. Primary Handling Editors: Madhura Mukhopadhyay, in collaboration with the *Nature Methods* team. Peer reviewer reports are available.

https://doi.org/10.1038/s41592-023-02037-0

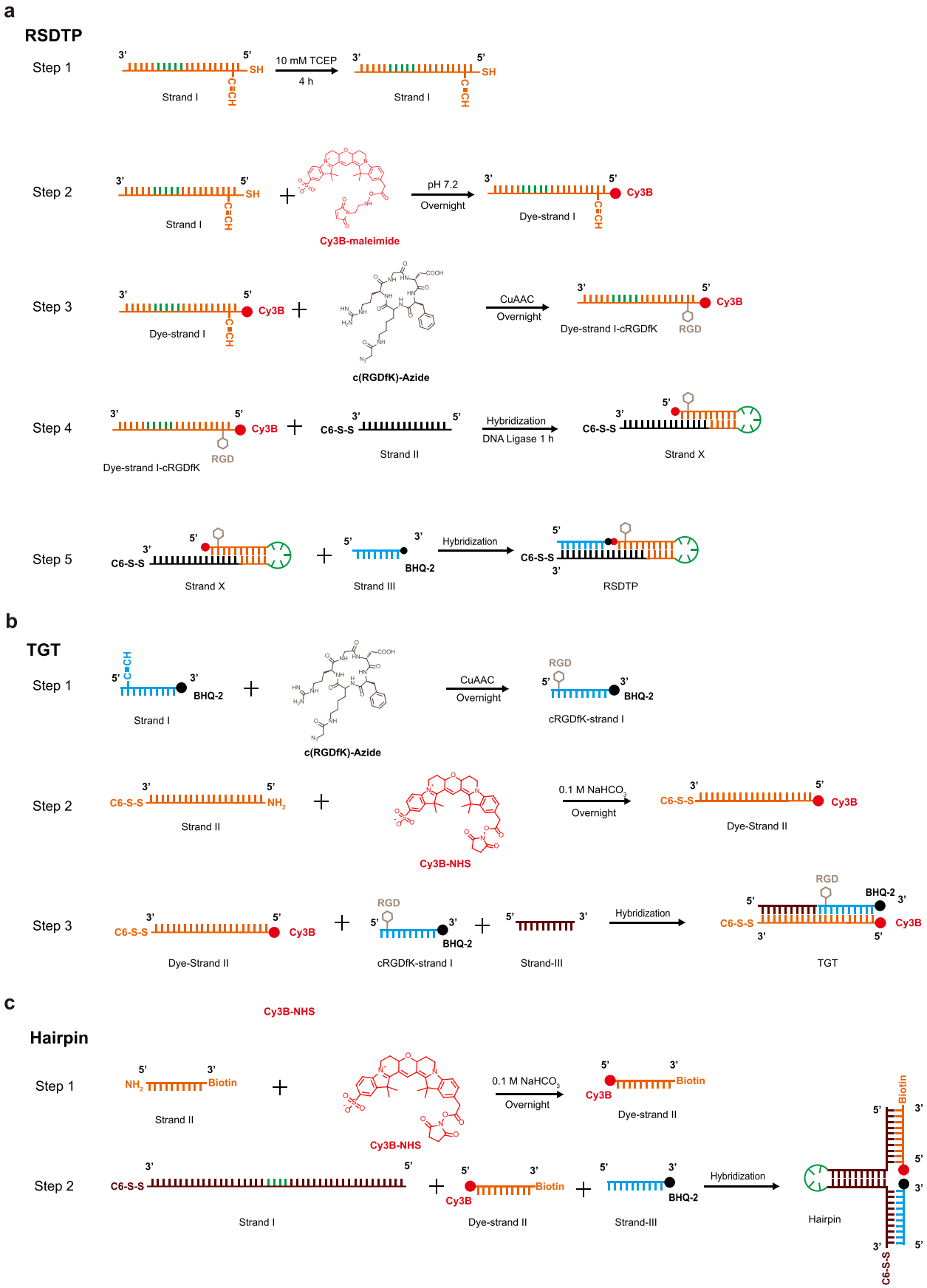

Extended Data Fig. 1 | Synthesis schemes of molecular tension probes. a, RSDTPs, **b**, TGTs and **c**, Hairpins.

https://doi.org/10.1038/s41592-023-02037-0

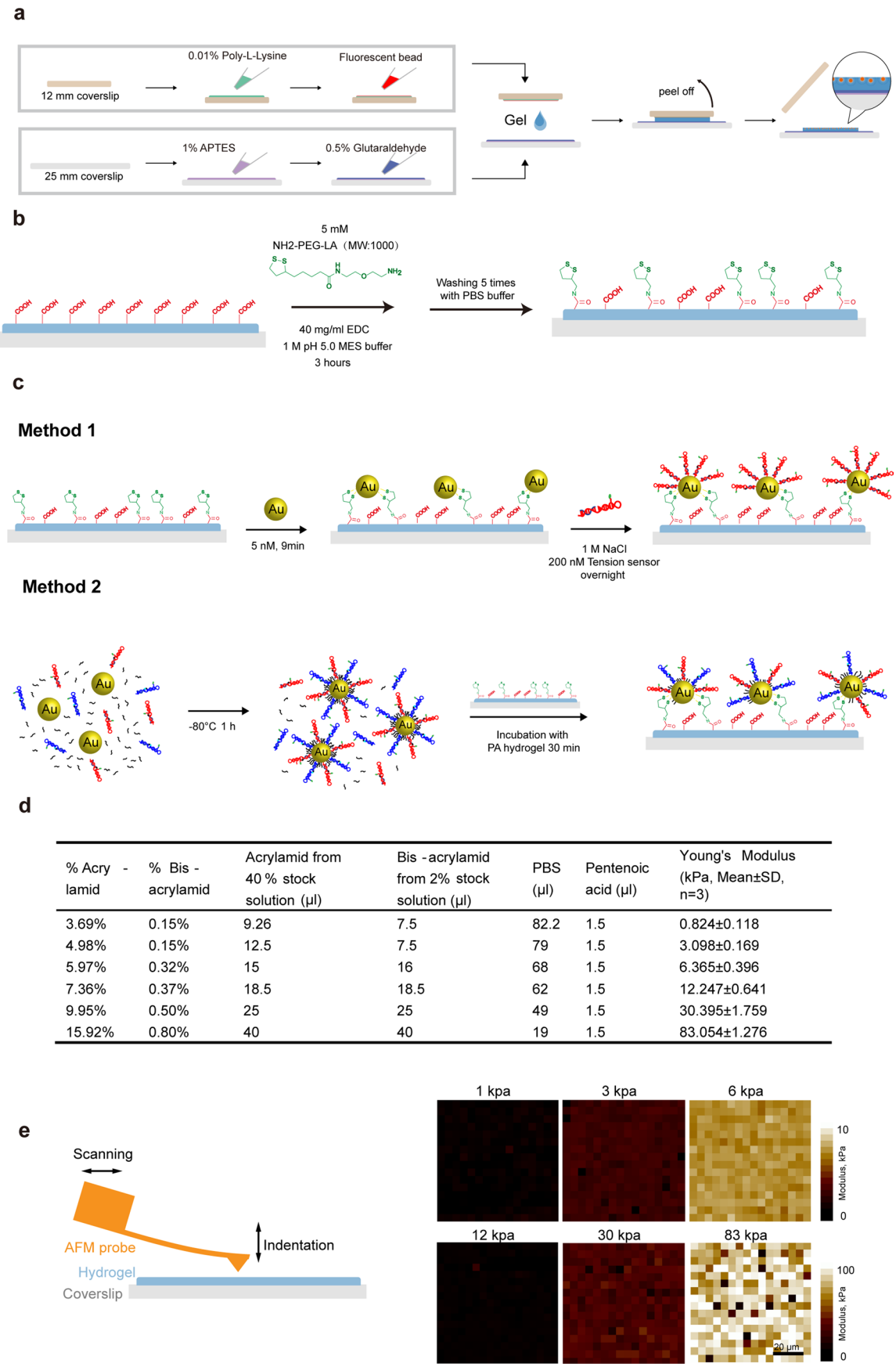

% Acry - lamid	% Bis - acrylamid	Acrylamid from 40 % stock solution (μl)	Bis - acrylamid from 2% stock solution (μl)	PBS (μl)	Pentenoic acid (μl)	Young's Modulus (kPa, Mean±SD, n=3)
3.69%	0.15%	9.26	7.5	82.2	1.5	0.824±0.118
4.98%	0.15%	12.5	7.5	79	1.5	3.098±0.169
5.97%	0.32%	15	16	68	1.5	6.365±0.396
7.36%	0.37%	18.5	18.5	62	1.5	12.247±0.641
9.95%	0.50%	25	25	49	1.5	30.395±1.759
15.92%	0.80%	40	40	19	1.5	83.054±1.276

Extended Data Fig. 2 | Development of PA hydrogel substrates functionalized with both TFM and mTFM. a, Immobilization of fluorescent nanobeads on the surfaces of prepared hydrogels for TFM. **b**, Introduction of lipo-acid groups into hydrogel network. **c**, Covalent attachment of DNA tension probes to hydrogel surfaces through Au NPs. **d**, Recipes of PA hydrogels with different stiffness (n = 3 samples) and, **e**, corresponding results of stiffness characterization using AFM (16 × 16 stiffness map within an 80 μm × 80 μm region of interest). The images are representative of three independent experimental results.

https://doi.org/10.1038/s41592-023-02037-0

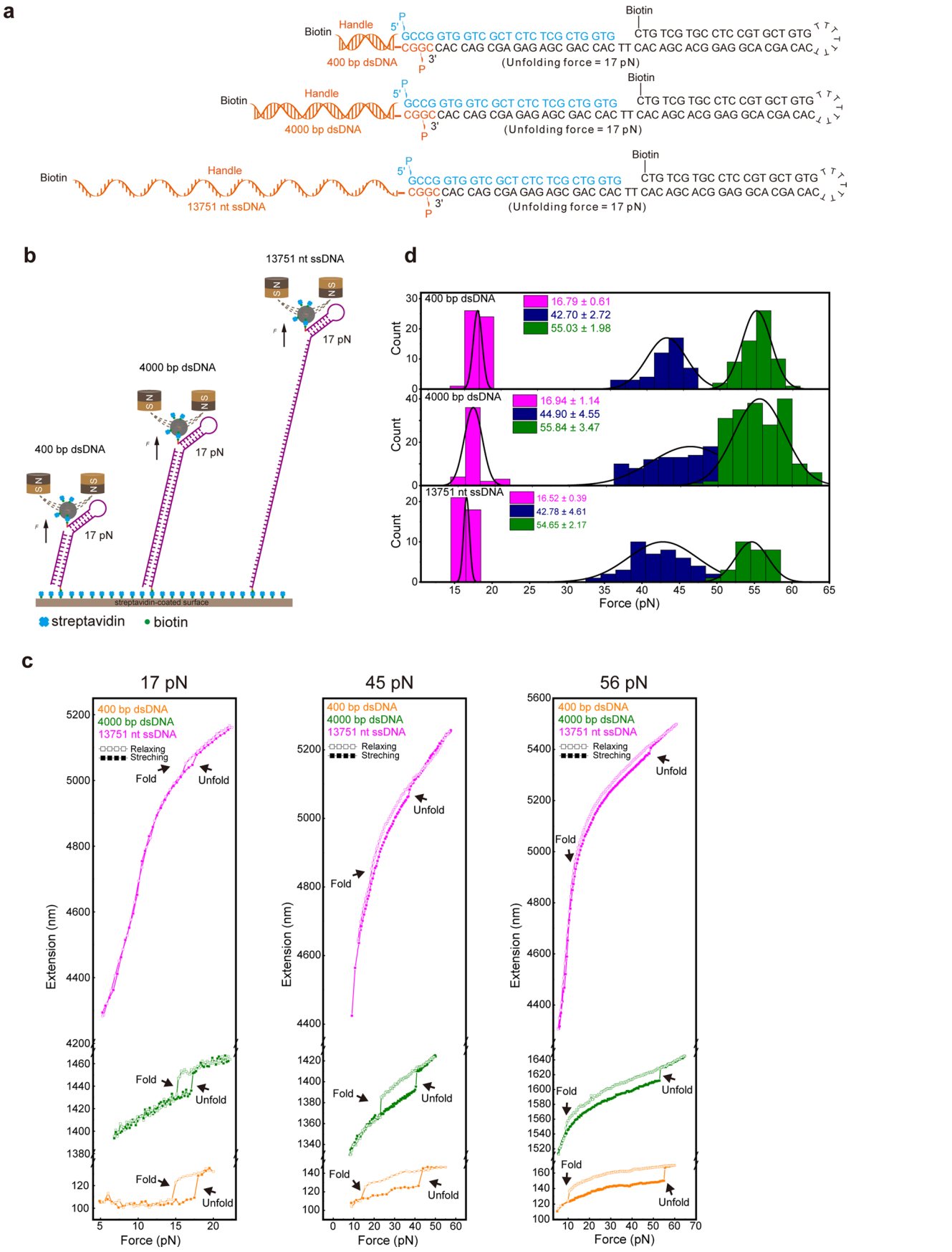

Extended Data Fig. 3 | Calibration of RSDTPs attached to handles with different stiffness using magnetic tweezer. a, Design and sequences of handles with different stiffness. **b**, Illustration of calibration setup using magnetic tweezer. **c**, Representative force-displacement calibration curves of 17 pN (left), 45 pN (middle), and 56 pN (right) RSDTPs. **d**, Distribution of unfolding forces of RSDTPs attached to handles with different stiffness (400 bp, n = 51, 46, 64 events for different RSDTPs. 4000 bp, n = 45, 121, 191 events for different RSDTPs. 13571 nt, n = 39, 45, 30 events for different RSDTPs).

https://doi.org/10.1038/s41592-023-02037-0

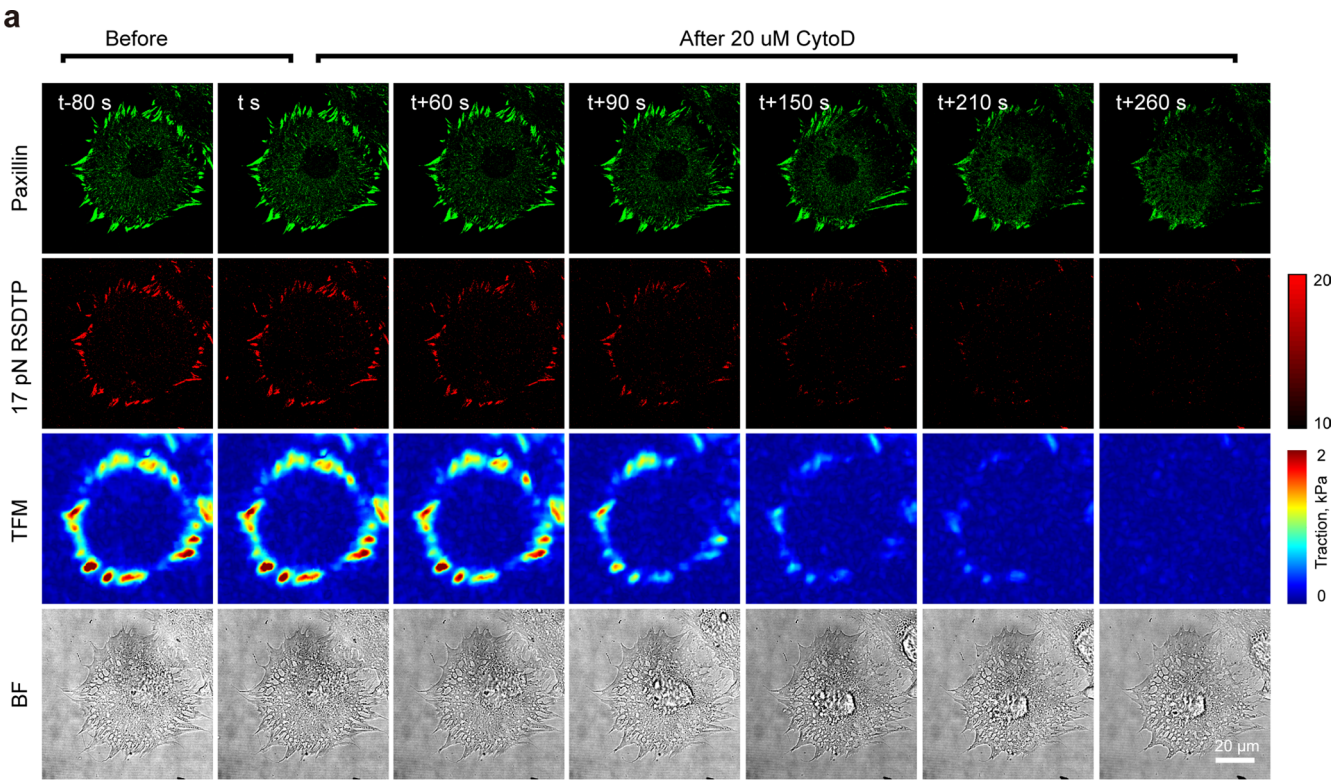

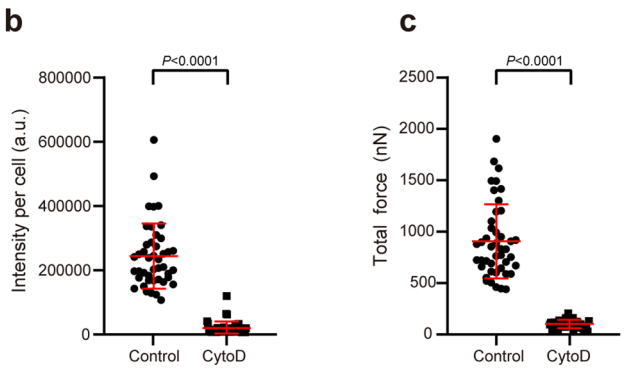

Extended Data Fig. 4 | Effects of CytoD on the mechanics of MEFs. **a**, Representative timelapse confocal imaging of paxillin-GFP, 17pN-RSDTPs, TFM of cells spreading on 30 kPa PA hydrogel before and after treatment of cytochalasin D (20 μM), and corresponding plots of **b**, total intensity of mTFM and **c**, total traction forces measured by TFM (Control, n = 44 cells. CytoD, n = 41 cells). Data represent mean ± s.d. of three experiments. Two-tailed Student t-test is used to assess statistical significance.

https://doi.org/10.1038/s41592-023-02037-0

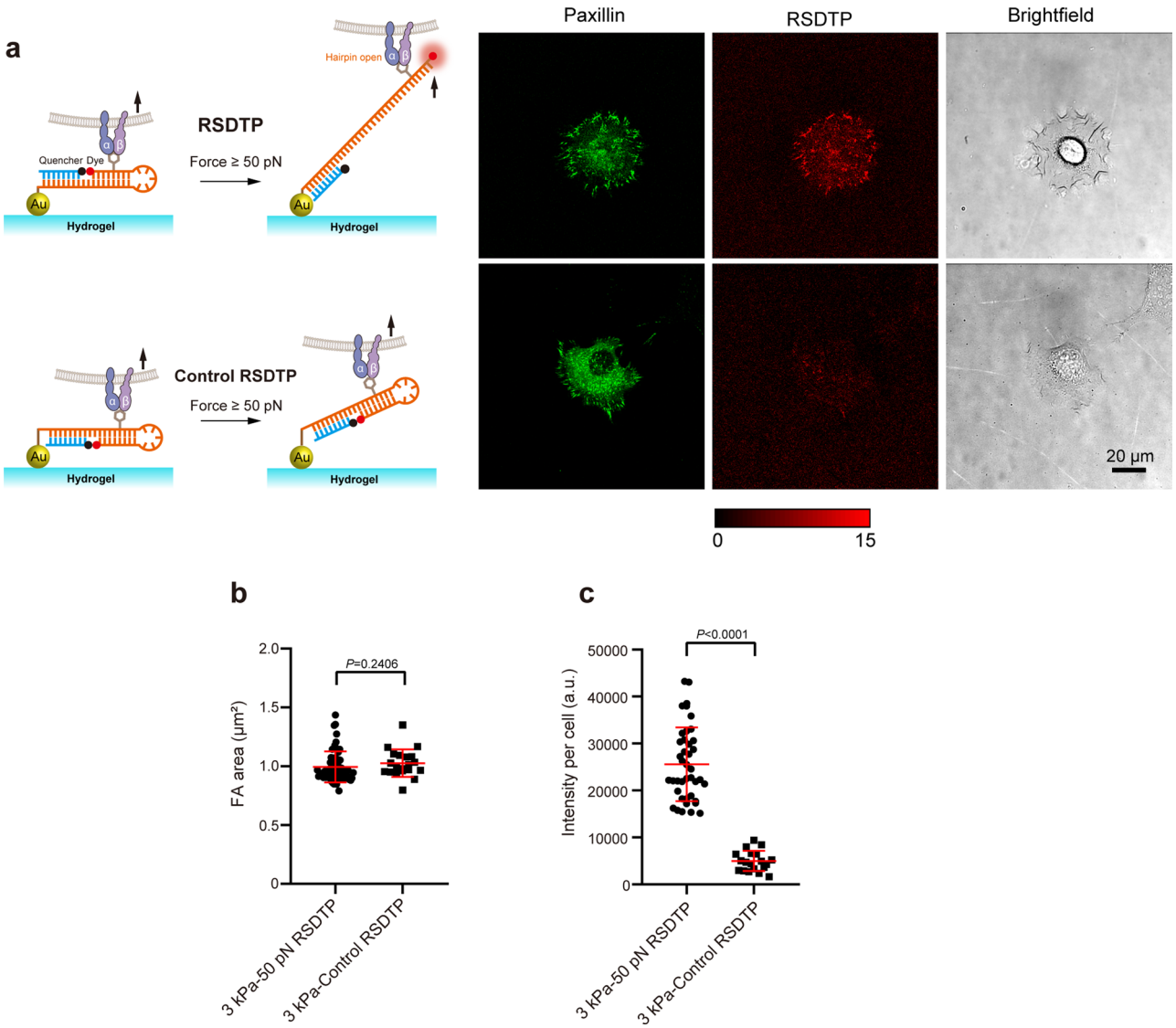

Extended Data Fig. 5 | The effect of gel deformation-induced aggregation of DNA tension probes on the validity of reported signals. a, Representative paxillin-GFP, mTFM and bright field images of cells incubated on 3 kPa PA hydrogel coated with a control RSDTP that was hardly unfolded and normal 50 pN RSDTP, and corresponding quantification of **b**, spreading area and **c**, integrin tensions signals (n = 41, 20 cells for each condition). Data represent mean± s.d. of three experiments. Two-tailed Student's t-test is used to assess statistical significance.

https://doi.org/10.1038/s41592-023-02037-0

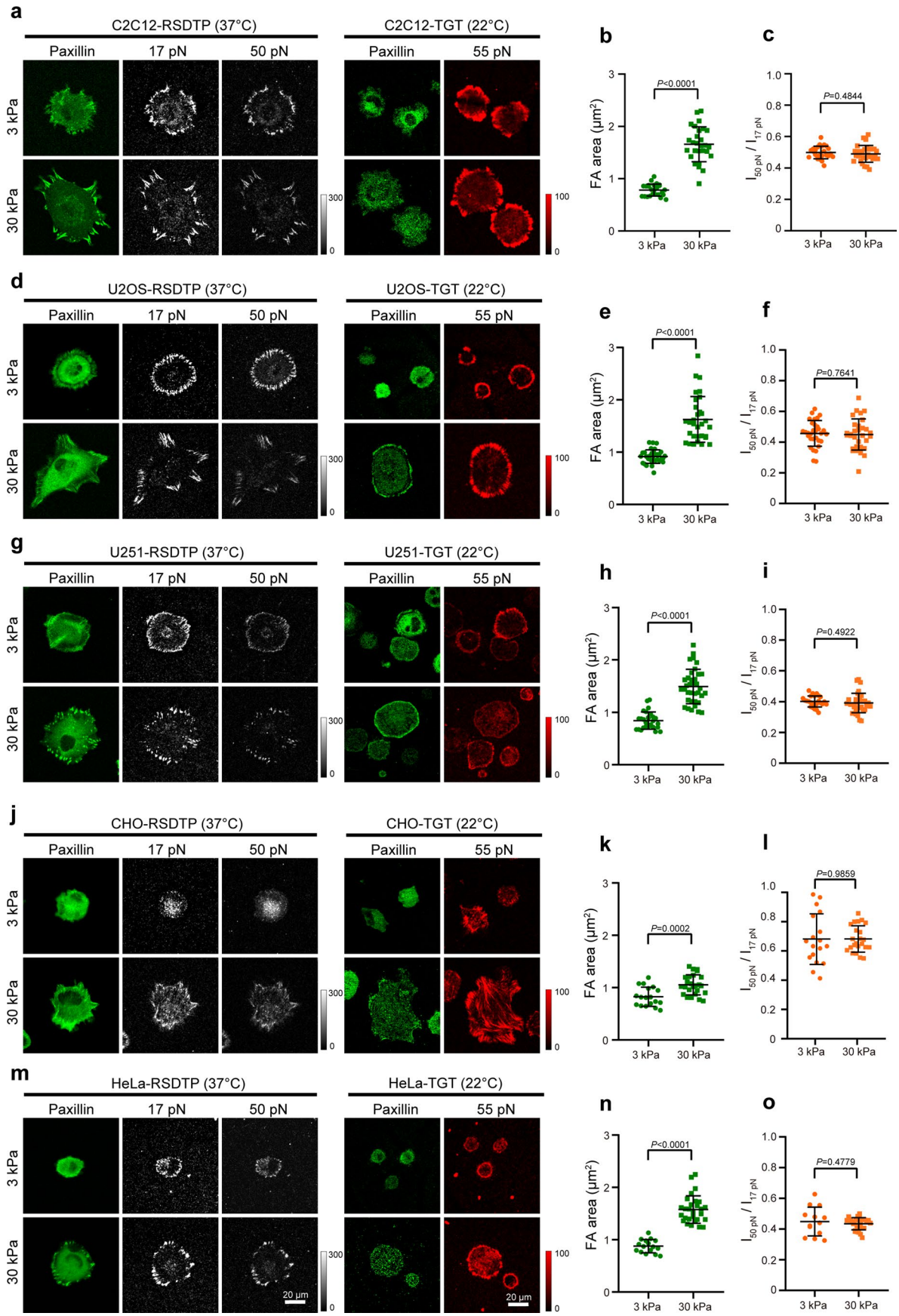

Extended Data Fig. 6 | See next page for caption.

https://doi.org/10.1038/s41592-023-02037-0

Extended Data Fig. 6 | Characterization of the integrin tension distribution of multiple cell lines on soft (3 kPa) and hard (30 kPa) hydrogels. Representative fluorescent images of paxillin-tagged **a**, C2C12, **d**, U2OS, **g**, U251, **j**, CHO, and **m**, HeLa cells on soft and hard hydrogel, and corresponding mTFM, simultaneously reported by mixed 17 pN-RSDTPs and 50 pN-RSDTPs at 37 °C (left), or 55 pN TGTs at room temperature 22 °C (right). The images are representative of three independent experimental results. FA area and the ratio of strongly loaded integrin to total loaded integrins of **b**, **c**, C2C12 (n = 25, 28 cells for each stiffness), **e**, **f**, U2OS (n = 31, 31 cells for each stiffness), **h**, **i**, U251 (n = 25, 34 cells for each stiffness), **k**, **l**, CHO (n = 18, 23 cells for each stiffness), and **n**, **o**, HeLa cells (n = 13, 28 cells for each stiffness) on soft and hard hydrogel. Data represent mean± s.d. of three independent experiments. Two-tailed Student's t-test is used to assess statistical significance.

https://doi.org/10.1038/s41592-023-02037-0

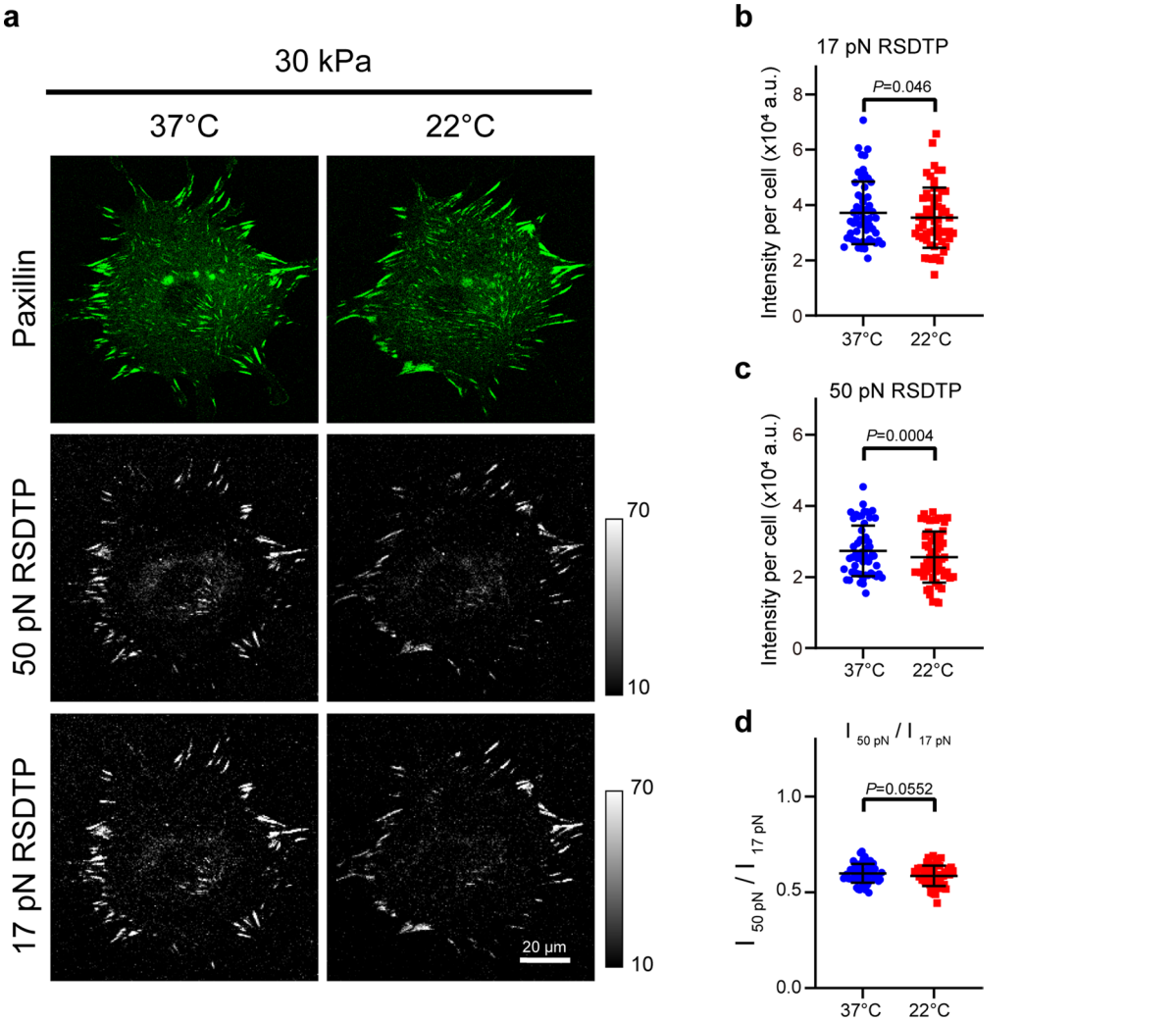

Extended Data Fig. 7 | Effect of temperature on mechanical stability of RSDTPs and associated results of hydrogel-based mTFM. a, Representative fluorescent images of paxillin-tagged MEFs on hydrogels (30 kPa) at 37 °C and room temperature (22 °C), and corresponding mTFM simultaneously reported by mixed 17 pN-RSDTPs and 50 pN-RSDTPs. Total intensity of mTFM per cell reported by **b**, 17 pN-RSDTPs, **c**, 50 pN-RSDTPs and **d**, their ratio (n = 56 cells). Data represent mean± s.d. of three independent experiments. Two-tailed Student's t-test is used to assess statistical significance. The insensitivity of force ratio to the ambient temperature indicates that even after mechanical stability of RSDTPs was diminished by the increase of temperature from room temperature (22 °C) to 37 °C, the absolute mechanical stability difference between 17 pN RSDTP and 50 pN RSDTP remains significant enough to characterize the distribution of integrin tension.

https://doi.org/10.1038/s41592-023-02037-0

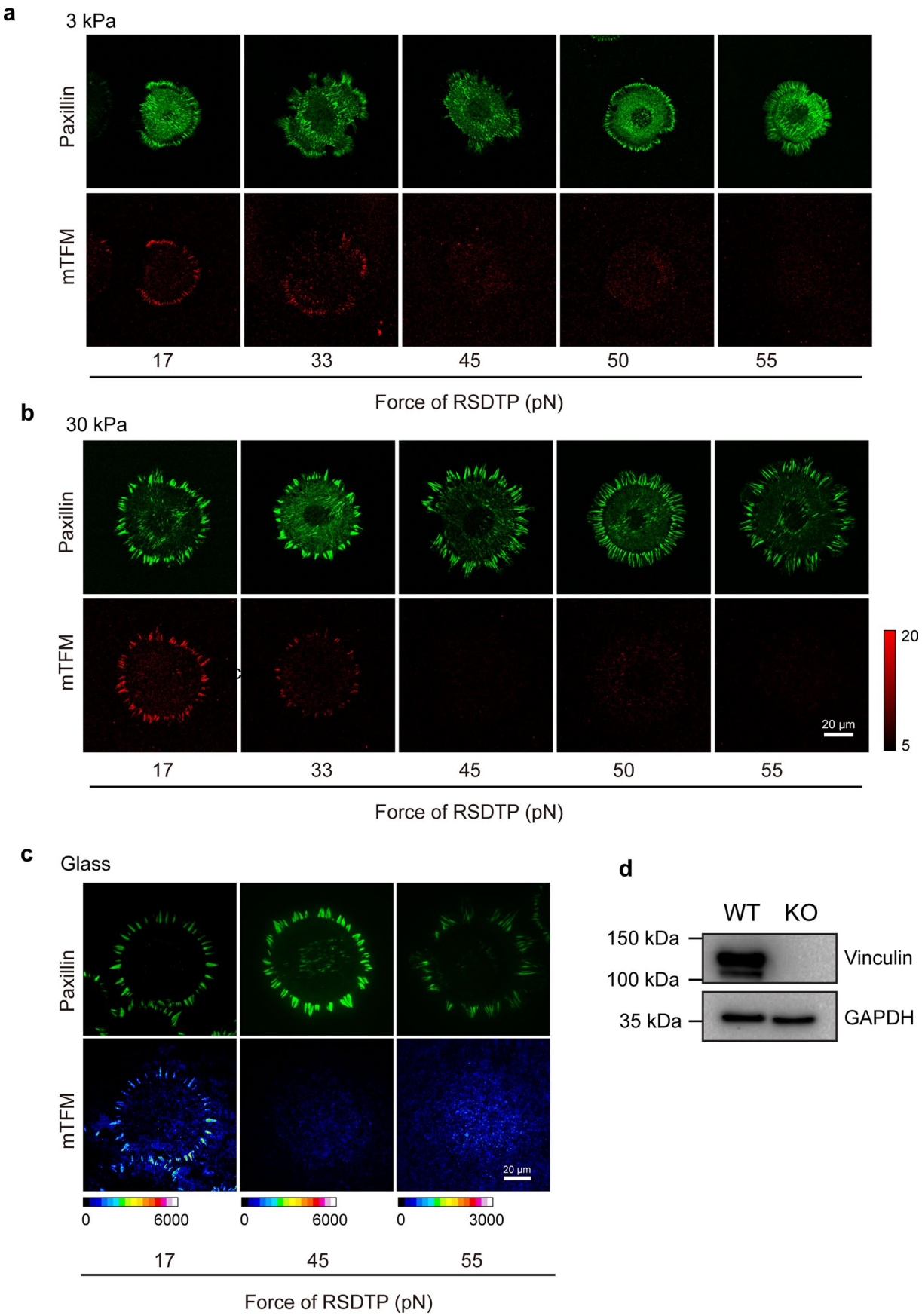

Extended Data Fig. 8 | The effect of substrate stiffness on integrin tension distribution of Vcl-KO MEF cells. Representative eGFP-paxillin and tension maps of different RSDTPs of Vcl-KO MEF cells on **a**, 3 kPa hydrogel, **b**, 30 kPa hydrogel, imaged using confocal microscope, and **c**, glass substrates imaged using TIRF. The images are representative of three independent experimental results. **d**, Western blot results of constructed Vcl-KO MEF cells. The gel images are representative of three independent experimental results.

https://doi.org/10.1038/s41592-023-02037-0

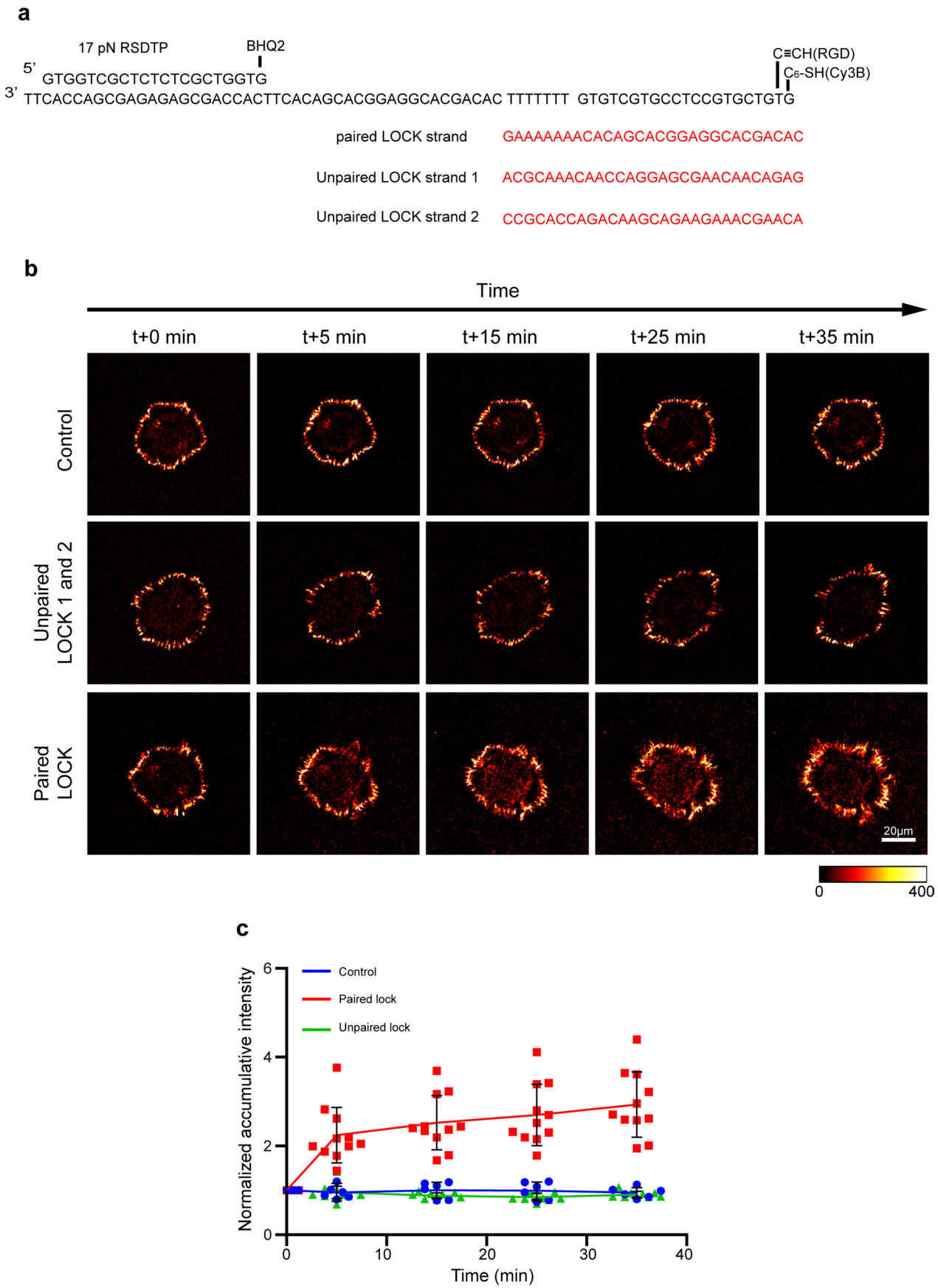

Extended Data Fig. 9 | See next page for caption.

https://doi.org/10.1038/s41592-023-02037-0

Extended Data Fig. 9 | The reliability of locking strands in tracing molecular tension. a. Sequences of 17pN-RSDTPs, paired locking strand, and unpaired locking strands. **b**, Representative paxillin-GFP and mTFM images of MEF cells plated on PA hydrogel with 17pN-RSDTPs in the absence of locking strands, after the addition of unpaired locking strands, and after addition of paired locking strands and **c**, corresponding plots of normalized accumulative intensity as a function of time (n = 6, 11, 9 cells for each condition). The images are representative of three independent experimental results. Data represent mean± s.d. of three independent experiments.

https://doi.org/10.1038/s41592-023-02037-0

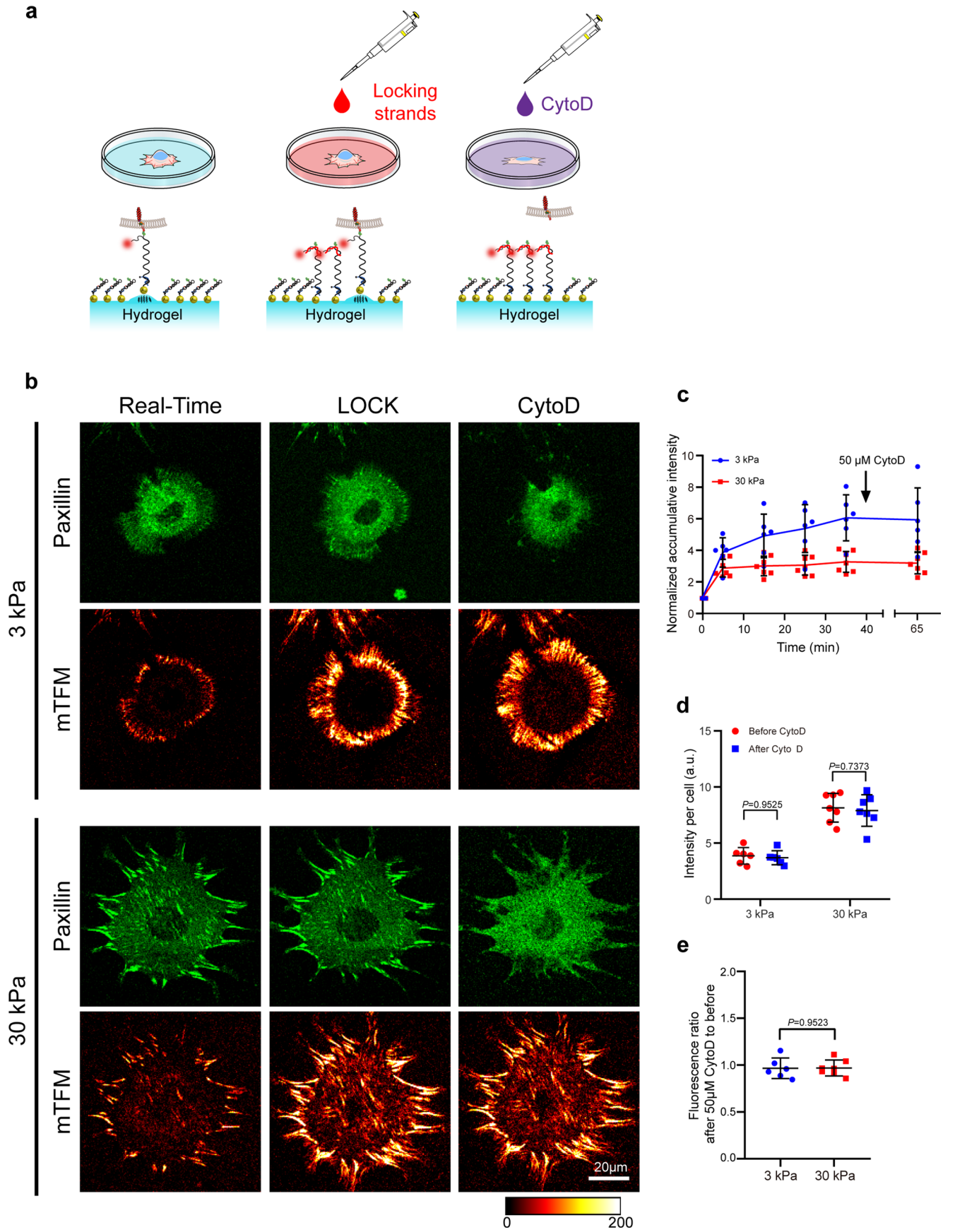

Extended Data Fig. 10 | See next page for caption.

https://doi.org/10.1038/s41592-023-02037-0

Extended Data Fig. 10 | Efficiency of locking strands in memorizing mTFM. **a**, Schematic diagram illustrating the flow of experiments. **b**, Representative Paxillin and mTFM images of MEFs seeded on 3 kPa and 30 kPa hydrogels functionalized with 50 pN RSDTPs before the addition of locking strands (left), after the addition of locking strands (middle), and after the treatment of Cytochalasin D (right), and corresponding **c**, plots of normalized accumulative intensity as a function of time (n = 6, 7 cells for each stiffness). The images are representative of three independent experimental results. Data represent mean± s.d. of three independent experiments. **d**, Total intensity of locked mTFM before and after the addition of CytoD and **e**, their ratios on 3 kPa and 30 kPa hydrogels (n = 6, 7 cells for each stiffness). Data represent mean± s.d. of three independent experiments. Two-tailed Student's t-test is used to assess statistical significance.

nature portfolio

Corresponding author(s): Zheng Liu

Last updated by author(s): Jul 21, 2023

Reporting Summary

Nature Portfolio wishes to improve the reproducibility of the work that we publish. This form provides structure for consistency and transparency in reporting. For further information on Nature Portfolio policies, see our Editorial Policies and the Editorial Policy Checklist.

Statistics

For all statistical analyses, confirm that the following items are present in the figure legend, table legend, main text, or Methods section.

n/a	Confirmed	
☐	☒	The exact sample size (*n*) for each experimental group/condition, given as a discrete number and unit of measurement
☐	☒	A statement on whether measurements were taken from distinct samples or whether the same sample was measured repeatedly
☐	☒	The statistical test(s) used AND whether they are one- or two-sided *Only common tests should be described solely by name; describe more complex techniques in the Methods section.*
☒	☐	A description of all covariates tested
☒	☐	A description of any assumptions or corrections, such as tests of normality and adjustment for multiple comparisons
☐	☒	A full description of the statistical parameters including central tendency (e.g. means) or other basic estimates (e.g. regression coefficient) AND variation (e.g. standard deviation) or associated estimates of uncertainty (e.g. confidence intervals)
☐	☒	For null hypothesis testing, the test statistic (e.g. *F*, *t*, *r*) with confidence intervals, effect sizes, degrees of freedom and *P* value noted *Give P values as exact values whenever suitable.*
☒	☐	For Bayesian analysis, information on the choice of priors and Markov chain Monte Carlo settings
☒	☐	For hierarchical and complex designs, identification of the appropriate level for tests and full reporting of outcomes
☒	☐	Estimates of effect sizes (e.g. Cohen's *d*, Pearson's *r*), indicating how they were calculated

Our web collection on statistics for biologists contains articles on many of the points above.

Software and code

Policy information about availability of computer code

Data collection	Zeiss LSM 880, Leica TCS SP8, Olympus FV3000, and Nikon Eclipse Ti2 TIRF microscopes were used to collect fluorescent images. NanoDrop microvolume spectrophotometer (Thermo Fisher) was used to determine the concentration of DNA tension probes, Au NPs, and proteins. High resolution field emission transmission electron microscope (JEOL, JEM-2100) was used to determine the Au NPs size. Field emission Scanning Electron Microscopy (Zeiss, GeminiSEM 500) was used to quantify the density of Au NPs on hydrogels. Atomic Force Microscope (Bruker, BioScope Resolve) was used to characterize the Young's modulus of prepared hydrogels. Gel Doc XR+ System (Bio-Rad) was used to detect the western blot.
Data analysis	ImageJ 1.53t, Matlab R2019a, Graphpad Prism 8.3.0, Microsoft Excel 2019, Origin 9.0

For manuscripts utilizing custom algorithms or software that are central to the research but not yet described in published literature, software must be made available to editors and reviewers. We strongly encourage code deposition in a community repository (e.g. GitHub). See the Nature Portfolio guidelines for submitting code & software for further information.

Data

Policy information about availability of data

All manuscripts must include a data availability statement. This statement should provide the following information, where applicable:

- Accession codes, unique identifiers, or web links for publicly available datasets
- A description of any restrictions on data availability
- For clinical datasets or third party data, please ensure that the statement adheres to our policy

The raw image data generated and analyzed that support the findings of this study are available from the corresponding author upon reasonable request. Statistics source data for all figures and supplementary figures are provided with this paper.

Human research participants

Policy information about studies involving human research participants and Sex and Gender in Research.

Reporting on sex and gender	The work did not include any studies with human research participants
Population characteristics	The work did not include any studies with human research participants
Recruitment	The work did not include any studies with human research participants
Ethics oversight	The work did not include any studies with human research participants

Note that full information on the approval of the study protocol must also be provided in the manuscript.

Field-specific reporting

Please select the one below that is the best fit for your research. If you are not sure, read the appropriate sections before making your selection.

☒ Life sciences ☐ Behavioural & social sciences ☐ Ecological, evolutionary & environmental sciences

For a reference copy of the document with all sections, see nature.com/documents/nr-reporting-summary-flat.pdf

Life sciences study design

All studies must disclose on these points even when the disclosure is negative.

Sample size	No statistical methods were used to predetermine sample size. For all the experiments, the sample size was chosen based on similar experiments and literature reports (ref: 5, 11, 13, 15). When taking cell time-lapse images, considering the time of acquisition, 3-5 cells can provide sufficient information on adhesion dynamics (PMID: 24358855). For measurement of the fluorescence intensity of tension image, more than ten cells were used for analysis for each condition. For calibration of DNA probes, over 30 force-extension curves were used to statistics the average unfolding forces for each type of tension probe. For measurement of the activation level of T cells, more than 75 cells were used for analysis for each marker.
Data exclusions	For cell image, images where cells failed to adhere to the substrate were not photographed. Of note, for Supplementary Fig.5b, only focal adhesions with molecular tension probe fluorescence signal greater than mean±3 standard deviations from background were analyzed.
Replication	Attempts at replication were successful. The exact number of independent experiments are provided in the figure legends. Of note, for the vinculin knockout experiment, we obtained 6 single clones using the CRISPR/Cas9 knockout system, and mixed them for all cell experiments.
Randomization	All samples were randomly allocated into experiment groups. Of note, for cell experiments, the same batch of cells were collected for each condition and randomly divided into separate group during an independent experiment, and microscopy images were taken from random regions of the coverslip for each experimental condition. When primary T cells were extracted, we used 6-8 weeks of age, both male and female mice randomly to normalize for potential sex differences.
Blinding	No blinding was performed as there were no experimental groups in this study.

Reporting for specific materials, systems and methods

We require information from authors about some types of materials, experimental systems and methods used in many studies. Here, indicate whether each material, system or method listed is relevant to your study. If you are not sure if a list item applies to your research, read the appropriate section before selecting a response.

Materials & experimental systems

n/a	Involved in the study
☐	☒ Antibodies
☐	☒ Eukaryotic cell lines
☒	☐ Palaeontology and archaeology
☐	☒ Animals and other organisms
☒	☐ Clinical data
☒	☐ Dual use research of concern

Methods

n/a	Involved in the study
☒	☐ ChIP-seq
☒	☐ Flow cytometry
☒	☐ MRI-based neuroimaging

Antibodies

Antibodies used

Biotin anti-mouse CD3ε Antibody was useful for T cell activation purchased from Biolegend, Clone#: 145-2C11, Cat#: 100304, Lot#: B313367

Biotin anti-mouse CD28 Antibody was useful for T cell activation purchased from Biolegend, Clone#: 37.51, Cat#: 102103, Lot#: B261776

FITC anti-mouse CD69 Antibody was useful for detecting CD69 expressing purchased from Biolegend, Clone#: H1.2F3, Cat#: 104505, Lot#: B355151

Alexa Fluor® 647 anti-ZAP70 Phospho (Tyr319)/Syk Phospho (Tyr352) Antibody was useful for detecting phosphorylation of ZAP70 purchased from Biolegend, Clone#: 1503310, Cat#: 683705, Lot#: B326163

Vinculin Recombinant Rabbit Monoclonal Antibody was useful for detecting Vinculin kockout in Western Blot analysis purchased from Thermo Fisher, Clone#: 42H89L44, Cat#: 700062, Lot#: 1984886

GAPDH Loading Control Monoclonal Antibody was useful as protein loading control in Western Blot analysis purchased from Thermo Fisher, Clone#: GA1R, Cat#: MA5-15738, Lot#: VB286430

HRP-conjugated Goat Anti-Mouse IgG was useful as secondary antibody for Western Blot analysis purchased from Sangon Biotech, Cat#: D110087, Lot#: I720AA0013

HRP-conjugated Goat Anti-Rabbit IgG was useful as secondary antibody for Western Blot analysis purchased from Sangon Biotech, Cat#: D110058, Lot#: H926AA0026

YAP antibody was useful for detecting location of YAP purchased from Santa Cruz Biotechnology, Clone#: 63.7, Cat#: sc-101199, Lot#: G2821

Alexa Fluor 647-conjugated Goat anti-mouse IgG was useful as secondary antibody for Immunofluorescence purchased from Sangon Biotech, Cat#: D110109-0100, Lot#: I330AA0001

Validation

Biotin anti-mouse CD3ε Antibody: Each lot of this antibody is quality control tested by immunofluorescent staining with flow cytometric analysis.
Product Citation: Logan K Smith et al. 2018. Immunity. 48(2):299-312

Biotin anti-mouse CD28 Antibody: Each lot of this antibody is quality control tested by immunofluorescent staining with flow cytometric analysis.
Product Citation : Hoover AR, et al. 2022. Clin Transl Med. 12:e937.

FITC anti-mouse CD69 Antibody: Each lot of this antibody is quality control tested by immunofluorescent staining with flow cytometric analysis.
Product Citation: Sun L, et al. 2021. Cancer Cell. 39:1361.

Alexa Fluor® 647 anti-ZAP70 Phospho (Tyr319)/Syk Phospho (Tyr352) Antibody: Each lot of this antibody is quality control tested by intracellular immunofluorescent staining with flow cytometric analysis.
Product Citation: Klammt C, et al. 2015. Nat. Immunol. 16:961

Vinculin Recombinant Rabbit Monoclonal Antibody: This antibody reacts with Human Vinculin. Based on sequence similarity, reactivity to chimpanzee, Rhesus monkey, swine, equine, mouse, rat, bovine, and chicken is expected. Test material for western blotting/immunofluorescence: HeLa cells.
Product Citation: Haugen RJ, et al. 2022. J Biol Chem. 298(9):102270

GAPDH Loading Control Monoclonal Antibody: This antibody has been successfully used in Western blot, ICC, IF, IHC (P), FACS and ELISA.
Product Citation: Bressan C, et al. 2020. Elife. 9:e56006.

YAP antibody: This antibody has been successfully used in WB, IP, IF, IHC(P), ELISA.
Product Citation: Yavitt, FM. et al. 2023. Sci Adv. 9: eadd5668.

Eukaryotic cell lines

Policy information about cell lines and Sex and Gender in Research

Cell line source(s)	THP-1 (SCSP-648), CHO (SCSP-507), MEF (SCSP-105), U2OS (SCSP-5030), U251-MG (TCHu 58), C2C12 (SCSP-505) and Hela (SCSP-504) cells were purchased from Stem Cell Bank, Chinese Academy of Science. CD8 T cells were prepared from C57BL/6-Tg(TcraTcrb)1100Mjb/J mice.
Authentication	Cell lines were not authenticated.
Mycoplasma contamination	The cell lines were not tested for mycoplasma contamination.
Commonly misidentified lines (See ICLAC register)	No commonly misidentified cell lines were used.

Animals and other research organisms

Policy information about studies involving animals; ARRIVE guidelines recommended for reporting animal research, and Sex and Gender in Research

Laboratory animals	C57BL/6-Tg(TcraTcrb)1100Mjb/J mice were kindly provided by Prof. Yucai Wang lab (University of Science and Technology of China). These OT-I mice contain transgenic inserts for mouse Tcra-V2 and Tcrb-V5 genes. The transgenic T cell receptor was designed to recognize ovalbumin residues 257-264 in the context of H2Kb and used to study the role of peptides in positive selection and the response of CD8+ T cells to antigen. Mice were maintained under specific pathogen free conditions (20-25°C temperature and 50%-60% humidity), and there were five mice housed in each standard cage under 12h-light and 12h-dark cycles while fed ad libitum with a standard chow diet. Before splenocytes were isolated, mice were anesthetized with carbon dioxide and sacrificed for cervical dislocation.
Wild animals	The study did not involve wild animals.
Reporting on sex	Animals of both sexes were analyzed in this study, and our finding is not only applied to one sex. We used 6-8 weeks of age, both male and female mice randomly to normalize for potential sex differences, and the information of their sexes has not been collected.
Field-collected samples	No field-collected samples were used in this study.
Ethics oversight	The animal protocols used for this study have been approved by the Institutional Animal Care and Use Committee, ABSL-3 Laboratory Institutional Biosafety Committee of Wuhan University (Animal Using Protocol: WP2020-08127).

Note that full information on the approval of the study protocol must also be provided in the manuscript.